



# A multi-analytical study of Bronze Age pottery from the UNESCO site of Al-Khutm (Bat, Oman)

Federico Bernardini<sup>1,2</sup> · G. Vinci<sup>2</sup> · D. Prokop<sup>3,4</sup> · L. Barro Savonuzzi<sup>5</sup> · A. De Min<sup>5</sup> · D. Lenaz<sup>5</sup> · F. Princivalle<sup>5</sup> · E. Cocca<sup>6</sup> · Zs. Kasztovszky<sup>7</sup> · V. Szilágyi<sup>7</sup> · I. Harsányi<sup>7</sup> · C. Tuniz<sup>2,1</sup> · M. Cattani<sup>8</sup>

Received: 10 March 2020 / Accepted: 29 May 2020 / Published online: 11 July 2020  
© Springer-Verlag GmbH Germany, part of Springer Nature 2020

## Abstract

The extensive investigation carried out in recent years at the UNESCO site of Al-Khutm (Ibri, Oman) has allowed to uncover the monumental remains of a tower dated back to the third millennium BC and to collect an abundant ceramic assemblage from the associated soil deposits. Eighteen selected pottery samples have been investigated using a multi-analytical approach including microfocus X-ray computed tomography, X-ray diffraction, optical microscopy and prompt gamma activation analysis to analyse the vessel-forming technique and to characterise their micro-structure, mineralogical and chemical composition to recognise possible local vs. non-local raw materials. The results provided new insights on ancient manufacturing processes and revealed that most of the vessels were locally produced exploiting raw materials from the surroundings of the site with the exception of a fragment of a black slipped jar. The chemical results suggest that the latter was imported from the Indus area in nowadays Pakistan. This evidence integrates our knowledge about the presence of this type of vessels in Oman and confirms the involvement of inland centres like Bat and Al-Khutm into a large-scale exchange system.

**Keywords** Bronze Age · Bat (Oman) · Tower · Pottery · Archaeometric analysis · Technology · Provenance

## Introduction

Located in north-western Oman within the inner region of the modern city of Ibri and registered as World Heritage Site by UNESCO, the tower of Al-Khutm represents one of the main archaeological complexes of the third millennium BC in the Arabian Peninsula (Fig. 1). The recent extensive investigation of the tower promoted by the Ministry of Heritage and Culture of Oman has allowed to uncover the monumental remains of

the tower and to collect an abundant ceramic assemblage from the deposit (Mantellini 2015; Cattani et al. 2017; Cocca et al. 2019).

Eighteen selected pottery samples from the above-mentioned site have been investigated using a multi-analytical approach in order to study the vessel-forming technique, often not clear at macroscopic level, and to characterise their micro-structure, mineralogical and chemical composition. All the pottery shards have been analysed by X-ray computed

---

**Electronic supplementary material** The online version of this article (<https://doi.org/10.1007/s12520-020-01099-x>) contains supplementary material, which is available to authorized users.

---

✉ Federico Bernardini  
fbernard@ictp.it

<sup>1</sup> Centro Fermi, Museo Storico della Fisica e Centro di Studi e Ricerche Enrico Fermi, Piazza del Viminale 1, 00184 Rome, Italy

<sup>2</sup> Multidisciplinary Laboratory, The Abdus Salam International Centre for Theoretical Physics, Strada Costiera 11, 34014 Trieste, Italy

<sup>3</sup> CEITEC-Central European Institute of Technology, Purkyňova 123, 612 00 Brno, Czech Republic

<sup>4</sup> Institute of Physical Engineering, Brno University of Technology, Brno, Czech Republic

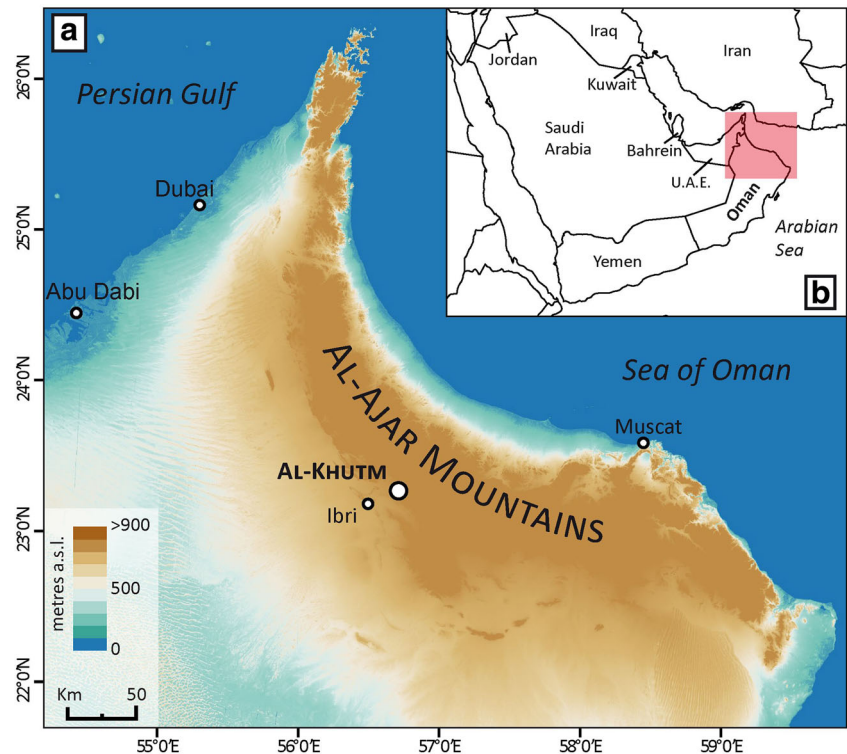
<sup>5</sup> Department of Mathematics and Geosciences, University of Trieste, Via Weiss 8, 34128 Trieste, Italy

<sup>6</sup> Associazione Internazionale di Studi sul Mediterraneo e l'Oriente, Corso Vittorio Emanuele II 244, 00186 Rome, Italy

<sup>7</sup> Nuclear Analysis and Radiography Department, Centre for Energy Research, Konkoly Thege 29-33, Budapest H-1121, Hungary

<sup>8</sup> Department of History and Cultures, University of Bologna, Piazza S.Giovanni in Monte 4, 40124 Bologna, Italy

**Fig. 1** Map of northern Oman and U.A.E. with the position of Al-Khutm (coordinates: 23.2798433 N, 56.7145780 E; **a**) and the Arabian Peninsula (**b**). DEM: ASTER NASA GDEM V3. Where not differently indicated, all maps are north-oriented



microtomography (microCT), optical microscopy (OM), X-ray diffraction (XRD) and prompt gamma activation analysis (PGAA). The results of all different techniques, providing a detailed description of pottery fabrics, have allowed to understand the technological process and whether the investigated vessels were locally produced or, at least part of them, imported from elsewhere, revealing important clues to reconstruct ancient exchange systems.

On the methodological side, the efficacy of non-destructive techniques, in particular the combined use of microCT and PGAA, has been tested by the integrated use of conventional methods (i.e. OM and XRD).

## Geographic, geological and archaeological background

The tower of Al-Khutm is located at about 3.5 km NW from the modern town of Bat within an oasis that extends for ca. 3.5 km<sup>2</sup> between the Wadi Ashwei and the Wadi Al-Hajar/Sharsah (Fig. 2). The latter is one of the major networks of south-flowing wadis coming from the central Al-Hajar mountain range.

The geology of the area is marked by the diffuse presence of ophiolitic and limestone occurrences which are the main components of the Al-Hajar Mountains, formed by the early Campanian (Late Cretaceous) thrusting of a fragment of the Tethys oceanic crust and the upper mantle over the north-eastern edge of the Arabian Platform and uplifted during the

Miocene Alpine orogeny. Gabbros with layered peridotites, sheeted dykes and pillow lavas compose the oceanic crustal sequence while the underlying upper mantle is mainly composed of harzburgites and dunite with chromitite pods (Lenaz et al. 2014; Soret et al. 2017). The high-temperature metamorphic sole is composed by amphibolite to granulite facies metabasalts while the low-temperature sole is composed by greenschist facies metacherts with imbrications of metatuffs and metasedimentary rocks (Soret et al. 2017). These mountains alternate with late Tertiary and Quaternary deposits deriving from the erosion of the range and resulted in piedmont scree and alluvial fans (Minoux and Jaujon 1986; Desruelles et al. 2016; Fig. 3).

Considering the archaeological background, the whole area of Bat is particularly rich in prehistoric evidences including several tower-like monuments, stone cairn tombs and settlement remains, many of them investigated from mid-1970s until recently (de Cardi et al. 1976; Frifelt 1975, 1985, 2002; Gentelle and Frifelt 1989; Brunswig 1989; Böhme 2011, 2012; Böhme and Al-Sabri 2011; Cable 2012; Döpfer and Schmidt 2014; Schmidt and Döpfer 2016; Döpfer 2018; Thornton et al. 2016: pp. 8–11 with refs). There is no doubt that Bat became one of the major centres of ancient “Magan”, i.e. the polity involved in the sea trade flourished in the south-eastern Arabian region during the third millennium BC according to the Mesopotamian texts (Cleuziou and Tosi 2007: pp. 139–157; Thornton et al. 2016: p. 161; Laursen and Steinkeller 2017). The outstanding

**Fig. 2** Geography of the area of Bat and Al-Khutm (modified from Google Maps, 2019)



concentration of building structures and the variety of goods found in this area suggest that a significant social and economic power was achieved by communities during this period.

As for other areas in the Arabian peninsula, this historical shift appears strictly connected to the emergence of the oasis agriculture (Cleuziou and Tosi 2007: pp. 151–155; Magee 2014: pp. 215–222) and based on cutting-edge water management systems including wells, cisterns, ditches and possibly underground or surface channels that enabled to transport the groundwater from the mountains to the floodplain (Charbonnier 2015; Desruelles et al. 2016; Cremaschi et al. 2018). Moreover, the whole area probably functioned as an important hub in the long-distance trade networks connecting the inland settlements, some of them specialised in the production and exploitation of important goods (e.g. copper, prestigious stones like the white marbled limestone and food

staple from crops and herds) with the coast and from here, in turn, with Mesopotamia, the Persian Gulf and the Indus valley (Cleuziou and Tosi 2007; Thornton and Schmidt 2015; Leigh 2016; Thornton et al. 2016).

Long-distance trade reached its peak in the second half of the third millennium BC, during the Umm an-Nar period (Early Bronze Age, 2800–2000 BC) and continue, possibly with minor intensity, in the following Wadi Suq period (Middle Bronze Age, 2000–1600 BC), according to the chronological system based on mortuary phases recognised in the south-eastern Arabian region (Cleuziou and Tosi 2007; Cleuziou 1989a, 1989b; Velde 2003; Thornton et al. 2016: pp. 2–4 and tab. 1.1).

The Wadi Suq period is marked by important social and economic changes over the whole region. This shift is indicated by consistent archaeological evidence such as the following: (1) the abandonment and/or reorganisation of several

**Fig. 3** Main geological units in the area of Ibri (adapted from Minoux and Jaujon 1986). Al, alluvial fans and alluvium (Late Tertiary-Quaternary deposits); Ar, Al-Ahrid formation, limestone and chert (Middle Triassic-Late Cretaceous); Sam, Ophiolites of the Samail Nappe (Late Cretaceous-Tertiary); Wa, Wahrah formation, lithoclastic, oolitic, marly limestone and chert (Upper Cretaceous)

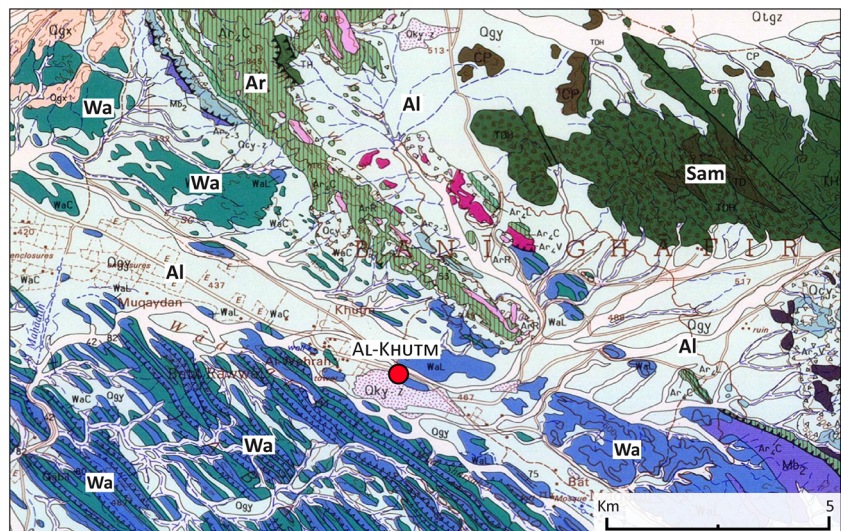


**Table 1** Description of pottery samples. *Inv.*, inventory; *Surf. treat.*: surface treatment; *Dec.*, decoration; *microCT*, microfocus X-ray computed tomography; *PGAA*, prompt gamma activation analysis; *XRD*, X-ray diffraction; *OM*, optical microscopy

| Sample n. | Inv. | Period         | SU  | Vase part | Munsell colour                        | Surf. treat. | Dec. | Wheel made | Shape             | Analytical methods     |
|-----------|------|----------------|-----|-----------|---------------------------------------|--------------|------|------------|-------------------|------------------------|
| 049       | 1510 | Wadi Suq?      | 494 | Wall      | 2.5YR 4/4 reddish brown               |              | No   | No         | undetermined      | microCT; PGAA; XRD; OM |
| 050       | 1464 | Umm an-Nar     | 559 | Rim       | 2.5YR 6/6 light red                   |              | Yes  | Yes        | Jar               | microCT; PGAA; XRD; OM |
| 051       | 795  | Wadi Suq       | 464 | Wall      | 2.5YR 4/8 red                         | Buff         | No   | No         | Jar               | microCT; PGAA; XRD; OM |
| 052       | 1125 | Wadi Suq       | 499 | Rim       | 2.5YR 7/6 light red                   | Buff         | Yes  | Yes        | Bowl              | microCT; PGAA; XRD; OM |
| 053       | 972  | Wadi Suq       | 464 | Wall      | 7.5YR 6/4 light brown                 | Slipped red  | Yes  | Yes        | Jar               | microCT; PGAA; XRD; OM |
| 054       | 1485 | Wadi Suq       | 494 | Rim       | 2.5YR 7/6 light red                   | Slipped red  | Yes  | Yes        | Beaker            | microCT; PGAA; XRD; OM |
| 055       | 594  | Wadi Suq       | 465 | Wall      | 2.5YR 4/2 weak red                    | White slip   | Yes  | No         | undetermined      | microCT; PGAA; XRD; OM |
| 056       | 1515 | Umm an-Nar?    | 494 | Wall      | 2.5YR 6/1 reddish grey                | Washed       | No   | Yes        | undetermined      | microCT; PGAA; XRD; OM |
| 057       | 1097 | Wadi Suq       | 499 | Wall      | 2.5YR 4/4 reddish brown               |              | Yes  | Yes        | undetermined      | microCT; PGAA; XRD; OM |
| 058       | 952  | Wadi Suq       | 511 | Wall      | 2.5YR 6/8 light red                   |              | Yes  | Yes        | Jar               | microCT; PGAA; XRD; OM |
| 059       | 648  | Wadi Suq       | 465 | Wall      | 2.5YR 6/6 light red                   | Buff         | Yes  | Yes        | Jar               | microCT; PGAA; XRD; OM |
| 060       | 1648 | Umm an-Nar     | 551 | Wall      | 2.5YR 7/4 light reddish brown         | Washed       | Yes  | Yes        | undetermined      | microCT; PGAA; XRD; OM |
| 061       | 677  | Wadi Suq?      | 479 | Wall      | 2.5YR 7/6 light red                   | Slipped red  | Yes  | Yes        | Jar               | microCT; PGAA; XRD; OM |
| 062       | 1639 | Umm an-Nar?    | 350 | Rim       | 2.5YR 6/8 light red, 5/1 reddish grey |              | No   | Yes        | Jar               | microCT; PGAA; XRD; OM |
| 063       | 978  | Wadi Suq       | 464 | Rim       | 5YR 5/1 grey                          | Slipped red  | Yes  | Yes        | Spouted jar       | microCT; PGAA; XRD; OM |
| 064       | 1154 | Wadi Suq       | 464 | Wall      | 7.5YR 5/4 brown                       | Slipped red  | Yes  | Yes        | Jar               | microCT; PGAA; XRD; OM |
| 065       | 1524 | Umm an-Nar?    | 494 | Wall      | 2.5YR 6/4 light red                   | Washed       | No   | Yes        | undetermined      | microCT; PGAA; XRD; OM |
| 066       | 1650 | Indus pottery? | 551 | Wall      | 2.5YR 5/8 red                         |              | No   | ?          | Black Slipped Jar | microCT; PGAA; XRD; OM |

**Fig. 4** Aerial picture of the Al-Khutm tower from S-W (top); general plan of the tower at the end of the 2017/2018 campaign (bottom). Pivots and thresholds are displayed in blue; limestone outcrops in brown; fireplaces in grey. Aerial picture and plan by Enzo Cocca and Giacomo Vinci



settlements stably occupied in the earlier period; (2) the replacement of earlier types of pottery, stone vessels and metalwork by new ones with distinctive craftsmanship and technology; (3) the substitution of monumental collective tombs with new grave types including subterranean or semi-subterranean single burials (Cleuziou and Tosi 2007: pp. 257–276; Magee 2014: pp. 182–189).

In this context, monuments like the Al-Khutm tower may have been tangible signs of the oasis leadership and of the prestige of the community (Cleuziou and Tosi 2007; Cable and Thornton 2013). The extensive investigation carried out between 2015 and 2018 at this site has allowed to unveil the remains of a 4-m-high circular tower, an imposing 2-m-high perimeter wall and several structures located inside the

tower, including several entrances, a deep well found in the central corridor and two rows of rooms on both sides (Fig. 4). All these structures were built using blocks of local limestones.

Two major phases of construction of the tower and related wall structures were identified. After the initial layout of the area with several small rooms arranged between the tower and the external perimeter wall, the whole external area was sealed by a vast landfill that reshaped the outer space on the western side of the tower into a wide terrace. Similarly, in the inner part of the tower, several structures originally built (among which wall structures, clay floorings and the central well) were later covered by superimposed features (Fig. 4). Despite the present lack of absolute chronological markers, the

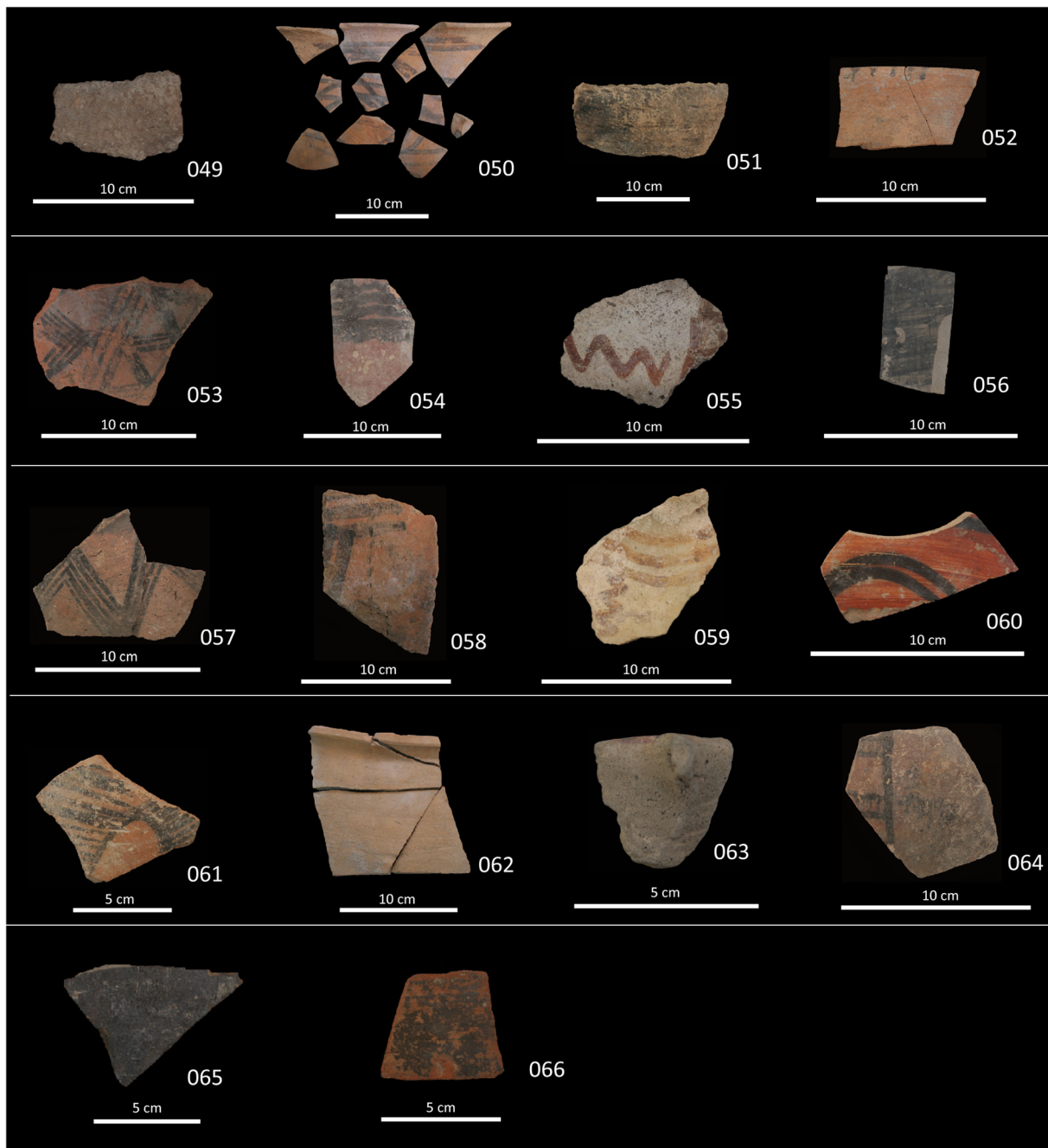


**Fig. 5** Pottery samples. Photos by Antonio Di Michele

preliminary analysis of pottery associated to the soil deposits suggests to ascribe the two major phases of construction/restoration to the Umm an-Nar and the Wadi Suq periods, respectively. According to such chronological span and to the shift in typological traits recognised in the ceramic assemblage, we tentatively propose that the tower was likely in use for long time, approximately between the second half of the third and the first half of the second millennium BC (Cocca et al. 2019).

## Materials and methods

In the present work, 18 shards found at Al-Khutm have been studied. Based on stratigraphic position and typological traits, 2 of them have been attributed to the Umm an-Nar period, 10 to the Wadi Suq period and a single fragment is perhaps part of a jar imported from the Indus area (Table 1). The attribution of the remaining 5 fragments is less certain. Nonetheless, 2 more shards can be cautiously

**Fig. 6** Drawings of selected pottery. Selected pottery vessels attributed to the Umm an-Nar period (050, 062) and to the Wadi Suq period (057, 059, 053, 063, 052, 054). Drawings by Ilenia Gennuso

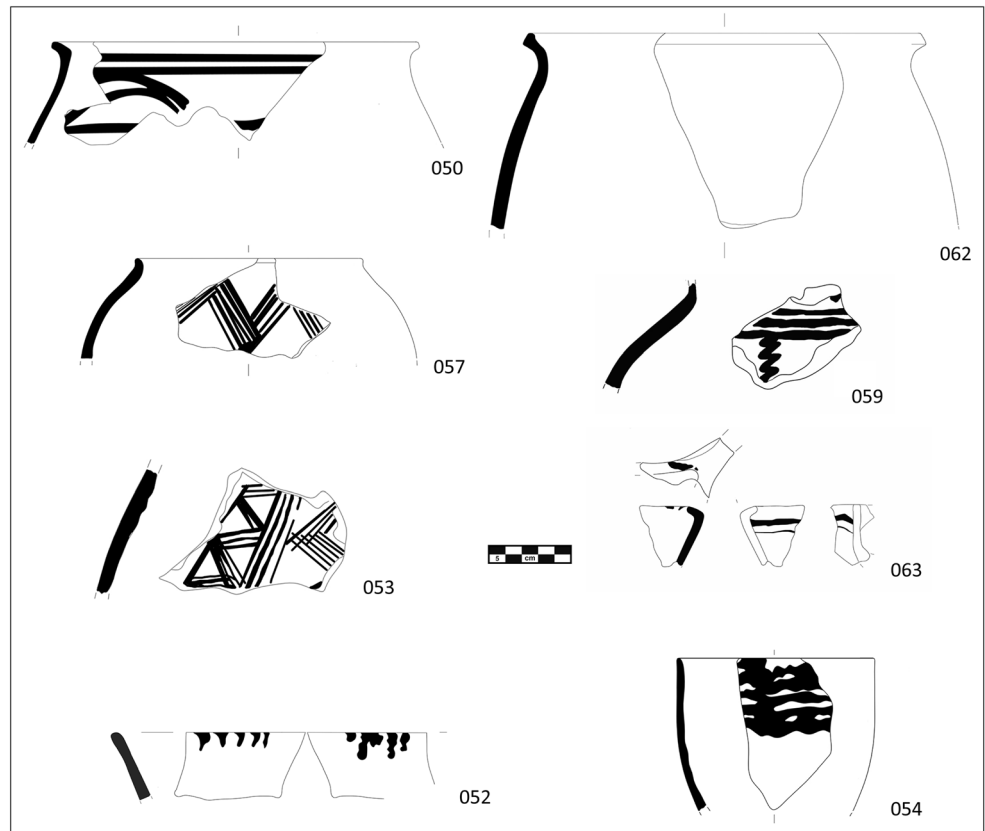
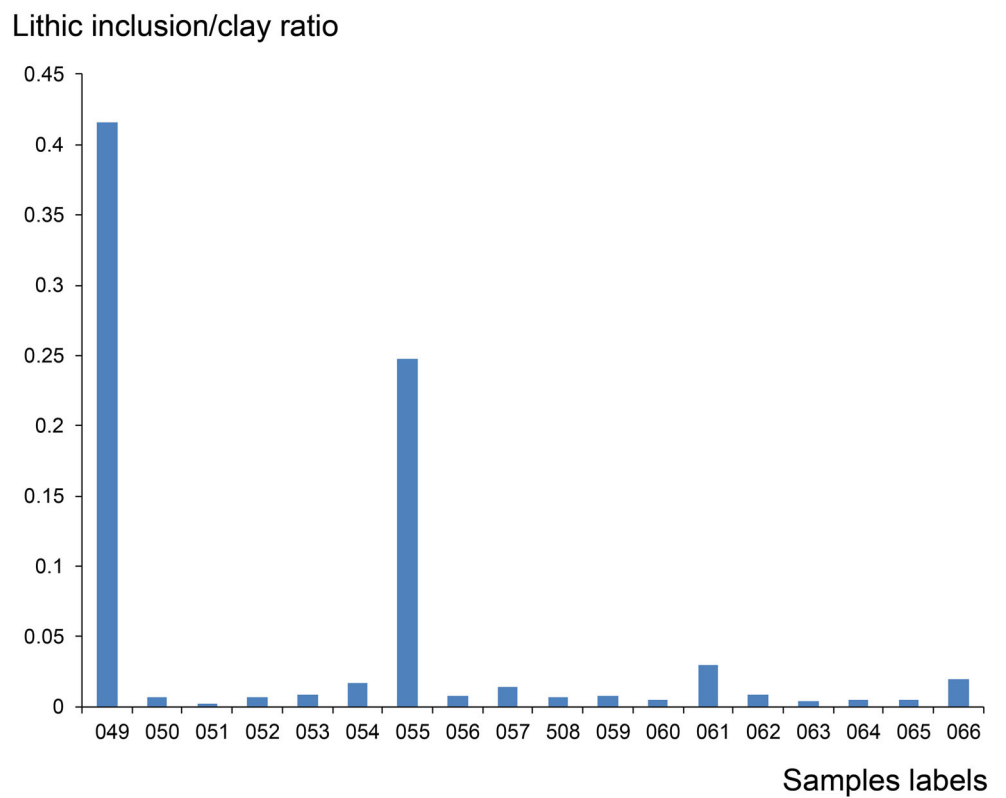


**Fig. 7** Lithic inclusion/clay ratio



referred to the Wadi Suq and 3 to the Umm an-Nar periods (Table 1; Supplementary Tab. 2).

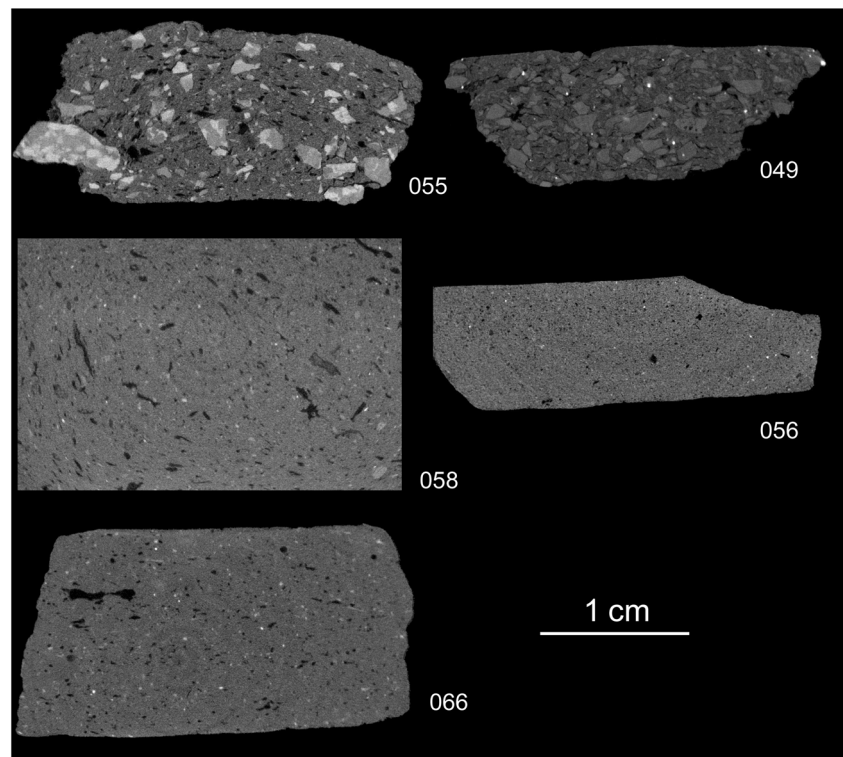
The sample of Umm an-Nar pottery is represented by shards belonging to oval or globular jars (050, 060; Figs. 5 and 6) with everted rims. Decoration is always black-painted and consists of horizontal thin parallel or curved lines under the rim and on the shoulder. These items can be compared with the homogeneous production identified at different sites (Hili, Bat, Amlah and Salut) and defined as “sandy red” for domestic usages. This specific ceramic production, despite having quite heterogeneous petrographic composition, is characterised by the constant association of a particular temper, technology and typological traits in shape and decoration (Méry 2000: pp. 125–168; Méry et al. 2017). Some good comparisons for jars come from settlement and funerary contexts in the area of Bat (Schmidt and Döpper 2016, fig. 3e and fig. 7d, f; Frifelt 1976, fig. 7) and from the tower of Hili 8 in the U.A.E. (period IIc2-f; Cleuziou 1989a, pl. 25, 8–12 and pl. 26, 7–8; Cleuziou 1989b, fig. 7, 1–4). Other pottery fragments have been cautiously attributed to the Umm an-Nar period according to their stratigraphic position, treatment of surface and decoration (056, 062, 065, Figs. 5 and 6).

A small pottery fragment with black slip and red fabric (066) is perhaps comparable with piriform jars typical of the Indus valley and well attested in Oman at several sites (Méry 2000: pp. 221–245; Méry et al. 2017) and also present in the area of Bat (Thornton et al. 2016, fig. 9.8B).

The Wadi Suq pottery sample is more consistent and include jars, spouted jars, bowls and beakers generally with slipped red or white surfaces. Among the close shapes, a fragment of globular jar (057) featured by the absence of the neck and having a vertical pointed rim is similar in shape and decoration to items found at Hili 8 period III (Righetti and Cleuziou 2010, fig. 5.13–14) and Shimal (Vogt and Franke-Vogt 1987, fig. 13, 9). Another very fragmented rim can be referred to a spouted jar with a black painted band on both sides (063), a peculiar type of Wadi Suq period (Carter 1997: p. 83; Righetti 2015: pp. 268–269; Méry 2000: pp. 254–255 and fig. 161, pp. 9–10).

The open shapes consist of bowls and beakers. Bowls have rectilinear walls decorated with small black-painted vertical drops on the rim (052) and find good comparisons with items from Hili 8 period III (e.g. Righetti and Cleuziou 2010, fig. 3.15). Cylindrical beakers, similar to that one here presented (054) and often decorated with painted lines under the rim, are a classic type of the Wadi Suq repertoire and well attested in both settlements and graves (Righetti 2015: pp. 263–264; Velde 2003: p. 104; Jasim 2012, fig. 8, 1–5). Beaker 054, decorated with wavy lines under the rim, is precisely comparable with an item from at Hili 8 (Righetti and Cleuziou 2010, fig. 1.1). Based on the decorative patterns (triangular motifs, wavy lines), other painted wall fragments (053, 055, 059, 061: Figs. 5 and 6) can be ascribed to the Wadi Suq period (Righetti 2015, figs. 111–113; Velde 2003, fig. 2).

**Fig. 8** Virtual sections of selected coarse-grained (049, 055), fine- (058, 066) and very fine-grained (056) vessels according to visual inspection





## Microfocus X-ray computed tomography

MicroCT can provide information about vessel-forming techniques and provenance of pottery materials (Kahl and Ramminger 2012; Sanger 2016; Machado et al. 2017; Kozatsas et al. 2018; Bernardini et al. 2016, 2019b). This technique is a precious non-destructive tool to perform fabric characterisation of pottery, allowing the visualisation and quantification of lithic inclusions, clay matrix, pores and discontinuities generally related to firing shrinkage, loss of organic temper or the result of how the vessels were shaped into their final form (Bernardini et al. 2016, 2019b). Discontinuities and pores within the paste can, in fact, give information about the pottery shaping techniques. Lindahl and Pikirayi (2010) have demonstrated that the orientation of pores within the ceramic body, from one wall surface to the other, can be used to distinguish vessel-forming techniques, in particular between U and N coiling and modelling techniques. The U coiling technique gives curved convex sub-parallel discontinuities, while N coiling technique produces sub-parallel pores with a diagonal orientation. In vessels produced by modelling techniques, the discontinuities are parallel to the wall surfaces.

The Al-Khutm vessels were analysed by X-ray microCT at the Multidisciplinary Laboratory of the “Abdus Salam” International Centre for Theoretical Physics (Trieste, Italy), using a system (Tuniz et al. 2013) specifically designed for the study of archaeological and paleoanthropological materials (e.g. Bernardini et al. 2012, 2016, 2018, 2019a, 2019b; Tuniz et al. 2012; Duches et al. 2019).

The microCT acquisitions of all specimens were carried out by using a sealed X-ray source (Hamamatsu L8121-03) at a voltage of 110 kV, a current of 90  $\mu$ A and with a focal spot size of 5  $\mu$ m. The X-ray beam was filtered by a 0.1-mm-thick copper absorber. A set of 1440 or 1800 projections of the artefacts were recorded over a total scan angle of 360° by a flat panel detector (Hamamatsu C7942SK-25, pixel size 50  $\mu$ m). The resulting microCT slices were reconstructed using the commercial software DigiXCT (DIGISENS) in 32-bit format and obtaining an isotropic voxel size of 12.75  $\mu$ m (Table 1).

## Segmentations

Using the Avizo v.8 software, three virtual sections for each sample, taken at the centre and at the edges of each data set, have been segmented in order to separate the clay matrix from the lithic temper materials and the pores following a procedure already applied by Bernardini et al. (2019b; see [Supplementary information](#)). After segmentation process, we have first calculated, using the same software, the total area of clay matrix, pores and lithic inclusions (including both temper material and lithic components within the raw material) for all three virtual sections selected for all the artefacts. The ratio between the

total area of different pottery components can give interesting insights on how the paste of the vessels was produced (e.g. Bernardini et al. 2016, 2019b).

However, as already discussed by Bernardini et al. (2019b), samples with a similar lithic inclusion/clay ratio could correspond to quite different pastes: the same ratio could be obtained considering a sample with very rare and big lithic grains or considering a vessel characterised by very abundant and small lithic inclusions. In order to overcome this bias, we calculated, using the Avizo v.8 software, the number, the area, the maximum length and the maximum width of every single lithic inclusion within the three selected virtual sections. After that, we summed up the results for each vessel, putting together the data obtained from the segmentation and analysis of the three virtual sections.

## MicroCT-derived data analysis

To manage the resulting huge amount of data, we have divided our datasets (values for area, maximum length and width of all inclusions) into four intervals using Matlab R2016b. The size of the intervals has been selected by taking into account the statistical distribution of each variable and, more specifically, their quartile values (Prokop 2018). This procedure was important to have the best representation of dimensional parameters describing the lithic inclusions within the paste, allowing a good separation between samples showing lithic grains of different sizes. As far as the area is concerned, the quartile values are 325  $\mu$ m<sup>2</sup>, 1137  $\mu$ m<sup>2</sup> and 4714  $\mu$ m<sup>2</sup>, and the intervals have been set as follows: very small inclusions, 0–325  $\mu$ m<sup>2</sup>; small inclusions, 325–1137  $\mu$ m<sup>2</sup>; medium inclusions, 1137–4714  $\mu$ m<sup>2</sup>; and big inclusions, bigger than 4714  $\mu$ m<sup>2</sup>. Considering the length, the quartile values are 28  $\mu$ m, 53  $\mu$ m and 108  $\mu$ m, and the intervals have been set as follows: very small, 0–28  $\mu$ m; small, 28–53  $\mu$ m; medium, 53–108  $\mu$ m; and big, larger than 108  $\mu$ m. As far as the width is concerned, the quartile values are 12  $\mu$ m, 38  $\mu$ m and 66  $\mu$ m, and the intervals have been selected as follows: very small, 0–12  $\mu$ m; small, 12–38  $\mu$ m; medium, 38–66  $\mu$ m; and big, larger than 66  $\mu$ m. The percentages of lithic inclusions falling within the defined size intervals have then been calculated (Table 2).

In order to extract the maximum information possible from the data, principal component analysis (hereinafter PCA; e.g. Jolliffe 2002) has been performed using programming language R (Kassambara 2017) and considering as variables inclusion/clay ratio and percentages of area, maximum length and maximum width. PCA is a multivariate analysis tool to reduce the dimensions of a given dataset. It is based on the idea of rotating the original coordinate system to a new one.

**Table 2** Percentage of lithic inclusions divided into four size intervals considering their area, maximum length and maximum width and the inclusion/clay ratio (Incl/Clay). *VS\_A*, very small area; *S\_A*, small area; *M\_A*, medium area; *B\_A*, big area; *VS\_L*, very small length; *S\_L*, small

length; *M\_L*, medium length; *B\_L*, big length; *VS\_W*, very small width; *S\_W*, small width; *M\_W*, medium width; *B\_W*, big width; *Incl/Clay*, inclusion/clay ratio

| Name | Area     |         |         |         | Length   |         |         |         | Width    |         |         |         | Material<br>Incl_Clay (%) |
|------|----------|---------|---------|---------|----------|---------|---------|---------|----------|---------|---------|---------|---------------------------|
|      | VS_A (%) | S_A (%) | M_A (%) | B_A (%) | VS_L (%) | S_L (%) | M_L (%) | B_L (%) | VS_W (%) | S_W (%) | M_W (%) | B_W (%) |                           |
| 049  | 5        | 17      | 32      | 46      | 7        | 20      | 27      | 46      | 9        | 25      | 21      | 45      | 41.5                      |
| 050  | 8        | 12      | 40      | 40      | 10       | 17      | 41      | 31      | 10       | 26      | 24      | 39      | 0.7                       |
| 051  | 9        | 23      | 42      | 25      | 14       | 23      | 42      | 21      | 14       | 32      | 30      | 24      | 0.2                       |
| 052  | 6        | 18      | 43      | 32      | 7        | 23      | 38      | 31      | 11       | 27      | 29      | 32      | 0.6                       |
| 053  | 4        | 9       | 32      | 55      | 5        | 14      | 31      | 51      | 6        | 16      | 25      | 54      | 0.8                       |
| 054  | 7        | 12      | 36      | 45      | 8        | 15      | 36      | 42      | 9        | 22      | 24      | 45      | 1.7                       |
| 055  | 6        | 12      | 32      | 49      | 8        | 16      | 28      | 48      | 9        | 20      | 23      | 48      | 24.8                      |
| 056  | 39       | 45      | 14      | 2       | 50       | 32      | 15      | 3       | 61       | 31      | 5       | 2       | 0.8                       |
| 057  | 7        | 22      | 38      | 32      | 9        | 26      | 33      | 32      | 13       | 30      | 25      | 32      | 1.4                       |
| 058  | 7        | 14      | 39      | 41      | 9        | 18      | 36      | 38      | 10       | 23      | 28      | 39      | 0.7                       |
| 059  | 42       | 26      | 24      | 8       | 46       | 27      | 20      | 7       | 51       | 28      | 14      | 7       | 0.7                       |
| 060  | 2        | 6       | 43      | 49      | 3        | 8       | 47      | 42      | 3        | 14      | 30      | 53      | 0.4                       |
| 061  | 36       | 20      | 27      | 17      | 33       | 25      | 24      | 18      | 36       | 31      | 15      | 18      | 2.9                       |
| 062  | 64       | 19      | 12      | 5       | 54       | 27      | 14      | 5       | 60       | 28      | 6       | 5       | 0.8                       |
| 063  | 7        | 8       | 37      | 48      | 7        | 13      | 34      | 46      | 7        | 19      | 27      | 47      | 0.4                       |
| 064  | 14       | 21      | 41      | 24      | 11       | 30      | 35      | 24      | 15       | 35      | 28      | 23      | 0.4                       |
| 065  | 6        | 19      | 36      | 39      | 6        | 26      | 34      | 35      | 10       | 25      | 26      | 39      | 0.5                       |
| 066  | 4        | 9       | 22      | 65      | 4        | 13      | 22      | 61      | 6        | 14      | 17      | 63      | 1.9                       |

The direction of the new axes is then chosen to explain the maximum variance within the dataset.

### X-ray diffraction

X-ray diffraction patterns of all investigated samples were obtained on powdered samples spread out on aluminium plates using a STOE D 500 X-ray diffractometer at room temperature at the Department of Mathematics and Geosciences of the Trieste University. CuK $\alpha$  radiation was used through a flat graphite crystal monochromator. The current and the voltage were set at 20 mA and 40 kV, respectively. The scanning angle ranged from 2 to 50° of 2 $\theta$ , steps were of 0.1° of 2 $\theta$ , and the counting time was of 2 s/step.

### Optical microscopy

Small samples have been extracted from all the investigated vessels, and they have been used to produce thin sections at the University of Padua. The thin sections have been observed via a polarising microscope at the Department of Mathematics and Geosciences of the University of Trieste.

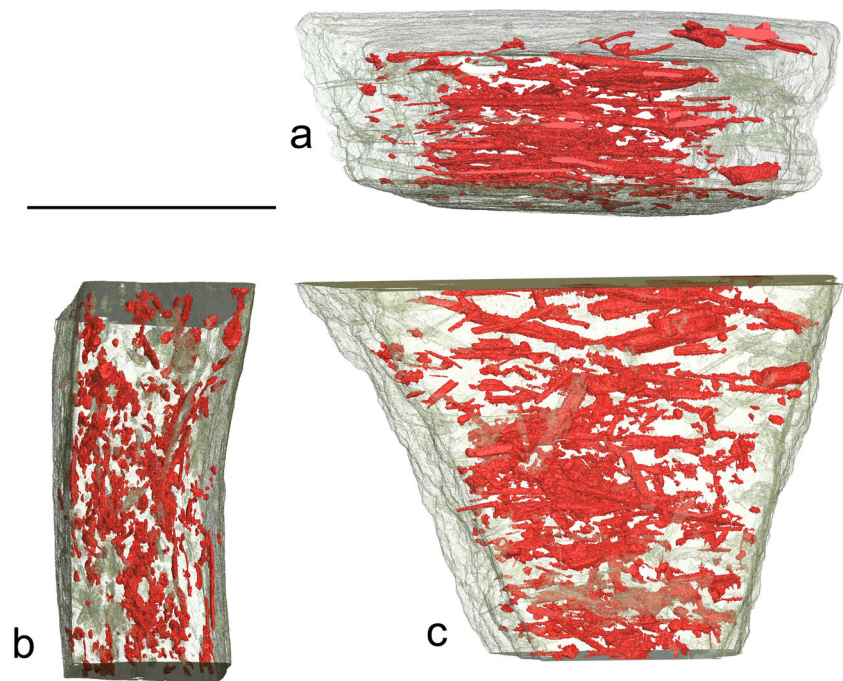
### Prompt gamma activation analysis

Even if the recent microCT analyses have given a good indirect fabric and technological characterisation of the investigated vessels (Bernardini et al. 2019b), PGAA data have been considered necessary to obtain an average bulk elemental composition of the samples useful to detail, confirm and/or correct the microCT, XRD and OM results.

PGAA is a method commonly used for the characterisation of archaeological materials (e.g. Kasztovszky et al. 2008, 2018; Bernardini et al. 2014a, 2014b, 2018, 2019a; Szakmány et al. 2011), including pottery. The first experiments to analyse archaeological pottery using internal monostandard method of PGAA were performed by Sueki et al. (1998). This study aimed to determine H, B, N, Si, Ca, Cd and Gd, which are difficult or impossible to measure by instrumental neutron activation analysis (INAA), to do provenance analysis. Since then, PGAA has been successfully applied to ceramic materials (Anderson 1995; Kasztovszky et al. 2004; Kasztovszky 2007; Szilágyi et al. 2012; Crupi et al. 2016; Palamara et al. 2016; Sekimoto et al. 2013; Leghissa et al. 2020).

It is accepted that PGAA enables to provide quantitative analytical data of the major (Si, Ca, Mg and Al) and minor (P,

**Fig. 9** MicroCT-derived rendering of the sample 52 with the clay paste in transparency and the pores in red. **a** Top view. **b** Lateral view. **c** Frontal view. Scale bar, 1 cm. Sub-parallel voids are elongated along the circumference of the vessel (**a**)



Cl, Na, K, Ti, Mn and Fe) components and only a few traces (B, Cr, Ni, Sm, Nd and Gd) with high neutron absorption cross-section. The data are considered as average concentration for the irradiated volume of a few tens of mm<sup>3</sup>, and supposed to be characteristic for the provenance of the clay.

The quantitative analysis of major elements and a few trace ones of all pottery samples have been carried out by PGAA at the Budapest Neutron Centre. The PGAA instrument operates at the horizontal cold neutron beam, characterised by a flux of  $9.6 \times 10^7 \text{ cm}^{-2} \text{ s}^{-1}$  (for the detailed description, see Szentmiklósi et al. 2010). PGAA is a non-destructive nuclear analytical method for quantitative determination of major and trace elements in samples of various physical and chemical forms. The method is based on the detection of characteristic gamma photons, emitted by atomic nuclei following neutron capture (Belgya and Révay 2004). Since neutrons can penetrate deep into the sample material, PGAA provides an average bulk composition for the irradiated volume of a few cm<sup>3</sup>. The prompt gamma spectra were collected by a Compton-suppressed HPGe detector, which has been accurately calibrated. The acquisition times have been set between 1900 and 5400 s, in order to achieve the statistically sufficient counts in the characteristic spectrum peaks for the determined elements. The gamma-ray spectra were evaluated using the Hypermet-PC programme (Révay et al. 2005). The quantitative analysis is based on the  $k_0$  principle (for a detailed description, see Révay 2009), using the spectroscopic data libraries developed at the Budapest laboratory (Choi et al. 2007). Both the self-absorption of prompt gamma photons due to the 20–30 cm thickness of the samples and the background from the blank measurement have been taken into

account. The accuracy of the results is lower than 3% and 10% for major and trace elements, respectively (Révay 2009).

## Results

### MicroCT

The segmentation of microCT datasets has allowed the virtual separation of the clay matrix, lithic inclusions and voids in 2D and their quantification. According to observations of microCT-derived virtual slices and the resulting lithic inclusions/clay ratios (Table 2; Fig. 7), two coarse-grained vessels have been recognised (049, 055; inclusion/clay ratio > 0.2) while all the other samples, regardless of their chronology and typology, are characterised by fine-grained pastes with a low inclusion/clay ratio (< 0.05). The coarse-grained sample 055, corresponding to an undetermined Wadi Suq vessel, shows abundant temper material with heterogeneous density with a size up to medium gravel (from < 1 to about 8 mm; lithic inclusion/clay ratio about 0.25). The coarse-grained sample 049, tentatively attributed to the Wadi Suq period too, is characterised by abundant low-density temper inclusions with a size up to fine gravel (from < 1 to about 3–4 mm; lithic inclusion/clay ratio about 0.4). The fine-grained vessels are variably tempered with lithic inclusions whose size is generally smaller than 1 mm. In sample 066, thin and elongated mineral inclusions (up to a few mm) likely corresponding to mica crystals are present (Fig. 8).

MicroCT data show that several vessels of both Umm an-Nar and Wadi Suq periods (Supplementary Fig. 1; vessels

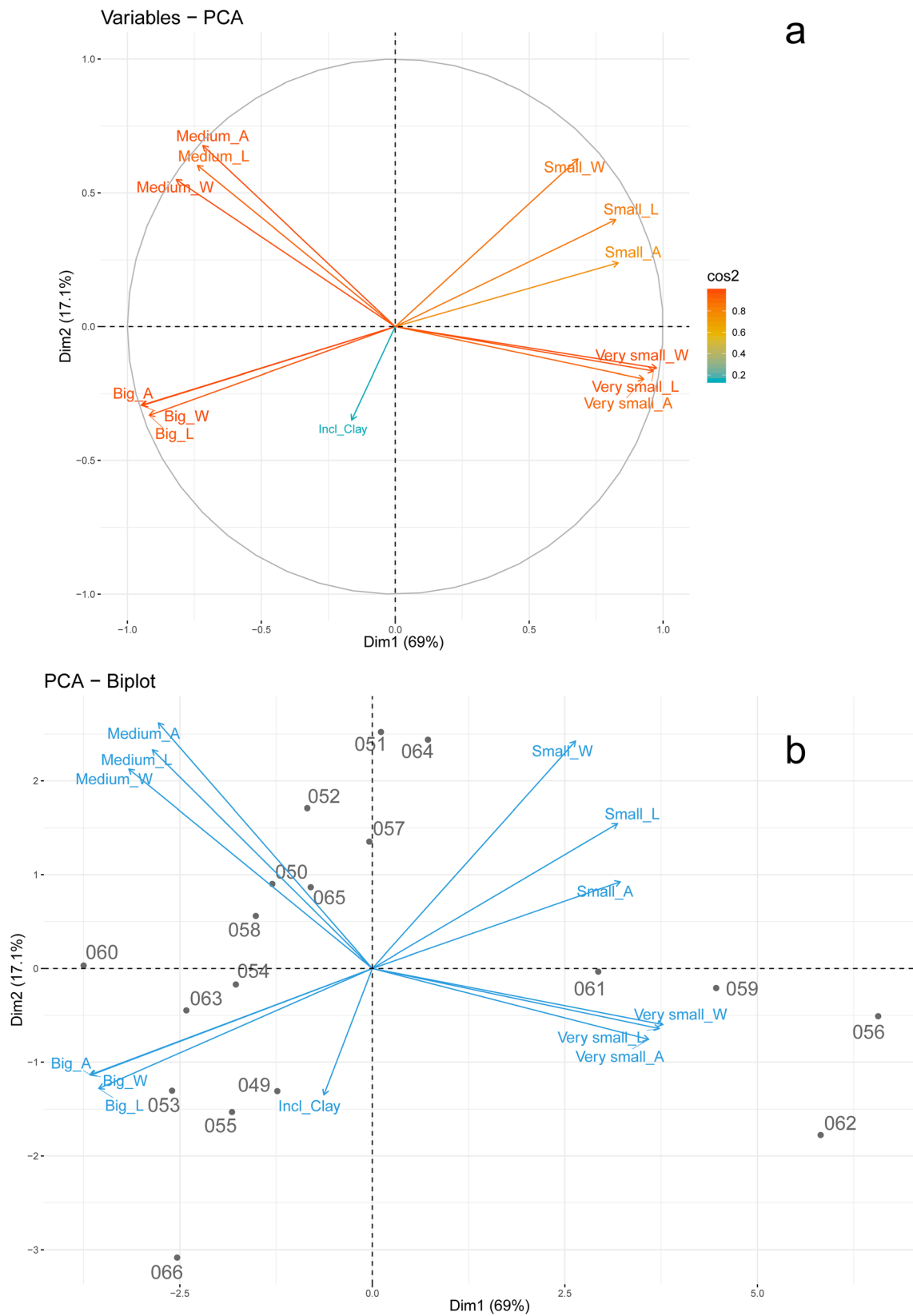


**Fig. 10** **a** Variable correlation plot showing the relationships among variables and the quality of their representation. **b** Bivariate plot showing the variables and the position of investigated samples. A, area; L, length; W, width; Incl\_Clay, lithic inclusion/clay ratio

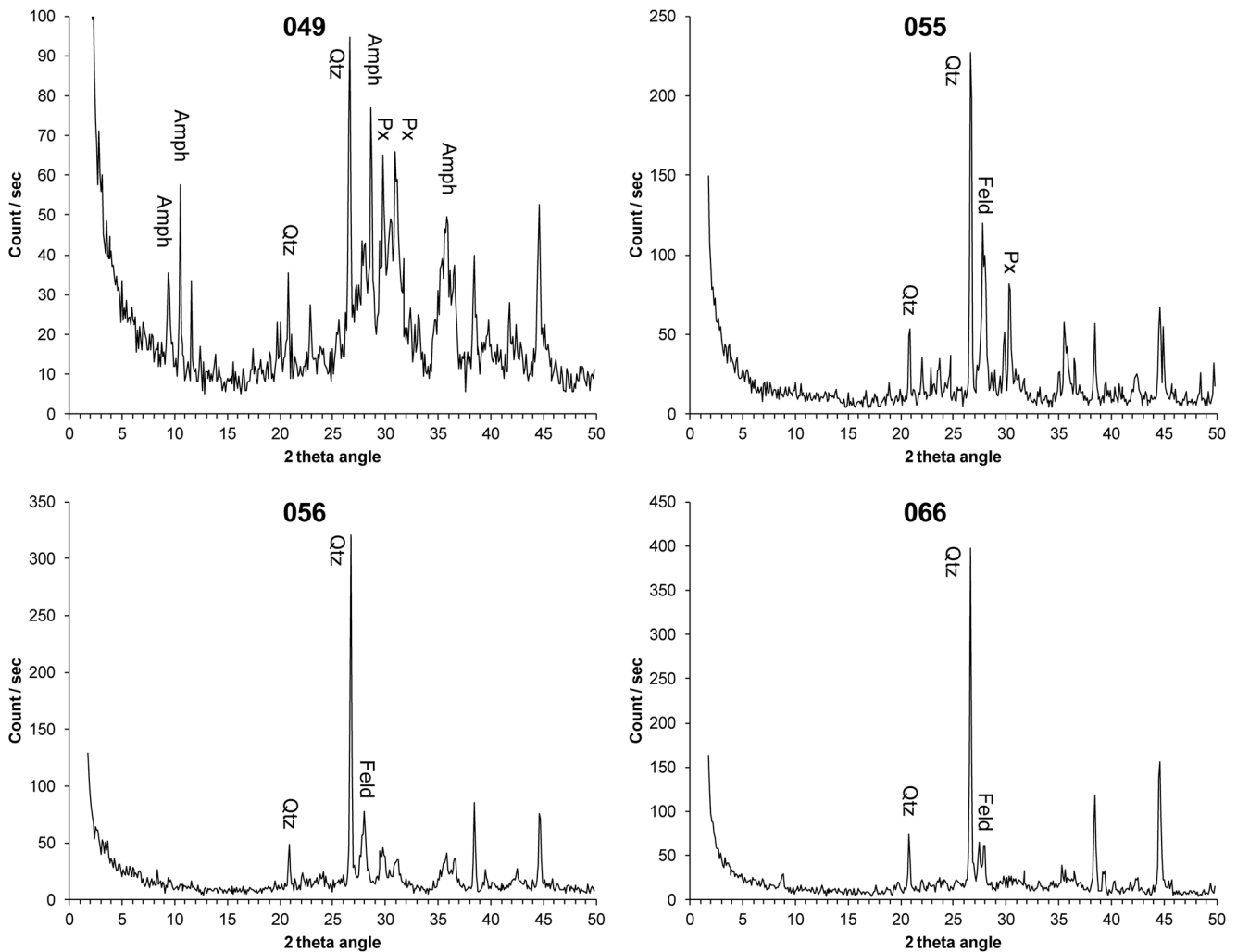


**Fig. 11** XRD spectra of selected samples. Amph, amphibole; Feld, feldspar; Px, pyroxene; Qtz, quartz

050–054, 056–057, 060–062, 064–066) have a paste with numerous elongated empty areas with sub-circular sections, corresponding to the spaces that were originally occupied by vegetal temper. Such voids are generally parallel to the wall surfaces and elongated along the circumference of the vessels (Fig. 9), confirming that the most of them were most probably produced using the wheel (e.g. Bordet and Courtois 1967; Rye 1977). No pores compatible with coiling or modelling techniques have been recognised (Lindahl and Pikirayi 2010). However, due to the small size of the investigated samples, it is not possible to exclude that at least part of them was not produced by wheel throwing but by wheel shaping of coil-built roughouts (Courty and Roux 1995; Méry et al. 2017). Such technique is well documented with slightly different variations at Umm an-Nar sites such as Salut and Hili (Méry 2000: p. 163; Méry et al. 2017: pp. 172–173).

After the segmentation of clay, lithic inclusions and pores in three slices per sample, we calculated the area, the

maximum length and the maximum width of every single lithic inclusion. Table 2 shows the percentages of lithic inclusions within the selected four size intervals considering their area, maximum length and maximum width.

To visualise and summarise the pottery fabric information given by microCT-derived data, PCA has then been performed considering data of Table 2 as input. Figure 10a shows the relationships between variables and the quality of their representation. Variables positively correlated are grouped together, while those negatively correlated are located in opposite quadrants. The quality of representation can be expressed by value of  $\cos^2$  (square cosine). The best representation of a variable is given when its end lies on the correlation circle, condition corresponding to the maximum square cosine value, that is 1. In Fig. 10a, variables are well represented and 4 main groups of variables are positively correlated: very small width - very small length - very small area; small width - small length - small area;

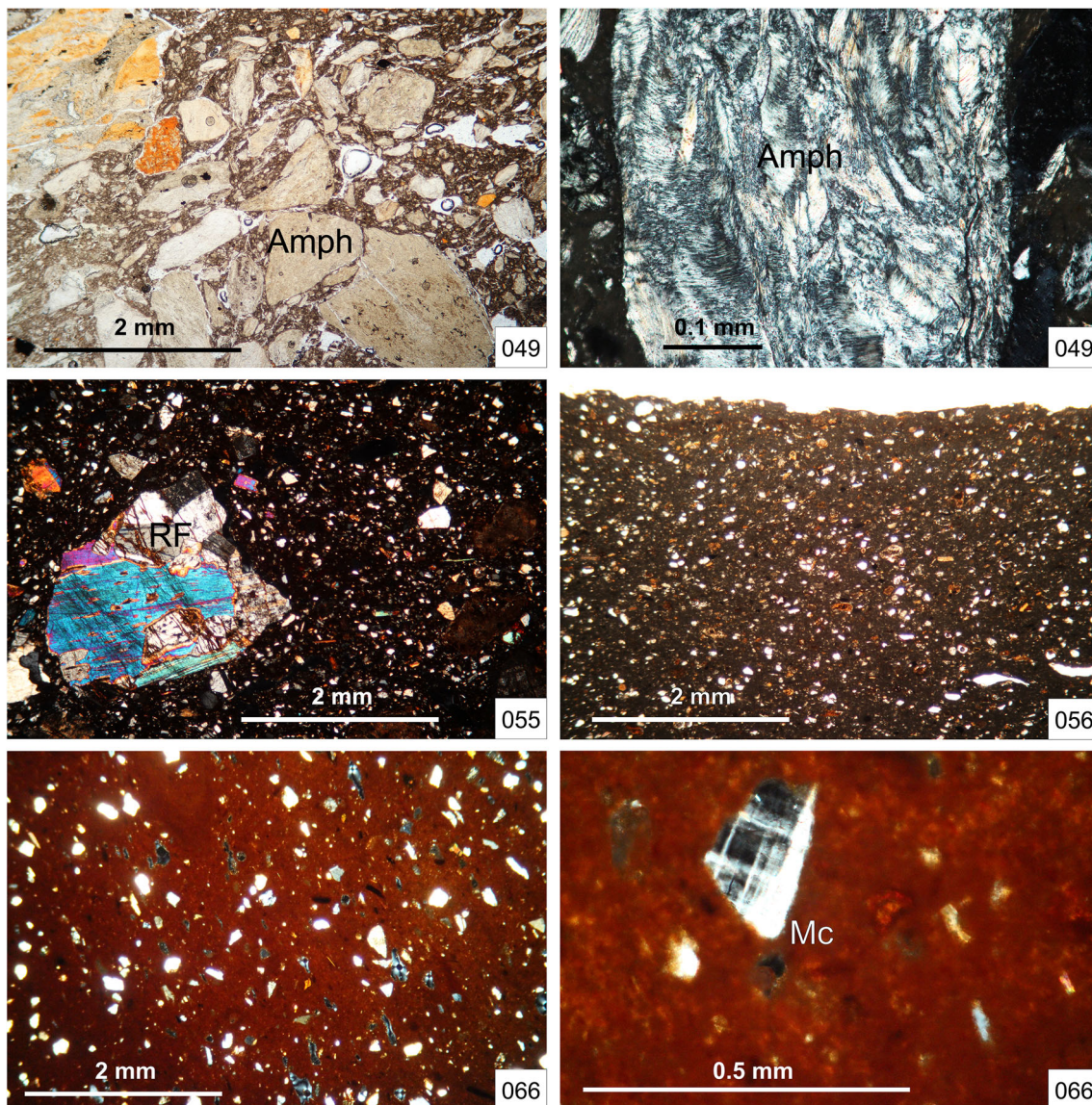


**Fig. 12** Microphotographs of thin sections of selected vessels. With the exception of the top left image, taken using plane-polarised light, all the others were taken using crossed polars. RF, rock fragment; Amph, amphibole; Mc, microcline

medium area - medium length - medium width; big area - big width - big length - inclusion/clay ratio.

A compact way to visualise the results of PCA is through a bivariate plot (Fig. 10b). In this plot, we can observe the position of the samples with respect to PC1 and PC2 and the variables. When a sample falls close to a given variable, it has a high value of such a variable, while its value is low if it is located on the opposite side of the same variable. Basically, it follows that when the samples are far away from each other, they are different. If points are grouped together, they are more similar. Just by visual inspection of the bivariate plot, three main groups of samples can be identified. Samples 056, 059, 061 and 062, falling in the bottom right quadrant, can be classified as samples with very small inclusions. Among them, sample 059 corresponds to a Wadi Suq jar, while the

other very fine-grained samples have been hypothetically attributed to both the Umm an-Nar (056 and 062) and Wadi Suq periods (061). Samples 049, 053 and 055 all attributed to the Wadi Suq period, fall in the bottom left quadrant and form a group characterised by coarse-grained pastes. Most of the samples, regardless of their chronology and typology, are clustered within or close to the top left quadrant including medium-grained pastes. Finally, sample 066, probably belonging to a jar imported from the Indus area, is well separated from all the other vessels, suggesting peculiar textural and technological features.

With the exception of sample 066, the results of PCA analysis do not reveal any significant typological-technological relationship. This result could be also related to the limited number of samples.

**Table 3** Major (wt%) and some trace (ppm) elements of the investigated vessels analysed by PGAA.  $Fe_2O_3$ , total Fe content. Data renormalized on a volatile-free basis. DL, detection limit

| Samples                        | 049   | 050   | 051    | 052    | 053    | 054   | 055   | 056   | 057   | 058   | 059   | 060   | 061   | 062   | 063    | 064   | 065   | 066   |
|--------------------------------|-------|-------|--------|--------|--------|-------|-------|-------|-------|-------|-------|-------|-------|-------|--------|-------|-------|-------|
| SiO <sub>2</sub> (wt%)         | 56.18 | 63.03 | 57.08  | 53.44  | 60.01  | 60.37 | 58.79 | 59.95 | 57.01 | 58.65 | 56.18 | 56.34 | 58.86 | 64.33 | 56.01  | 60.57 | 61.85 | 60.41 |
| TiO <sub>2</sub>               | 0.27  | 0.74  | 0.68   | 0.48   | 0.65   | 0.67  | 0.52  | 0.68  | 0.58  | 0.58  | 0.63  | 0.79  | 0.59  | 0.77  | 0.54   | 0.59  | 0.67  | 0.86  |
| Al <sub>2</sub> O <sub>3</sub> | 7.08  | 13.06 | 12.29  | 8.68   | 10.57  | 11.74 | 15.83 | 12.01 | 9.78  | 9.77  | 10.58 | 13.63 | 11.04 | 12.92 | 9.54   | 9.97  | 11.38 | 19.05 |
| Fe <sub>2</sub> O <sub>3</sub> | 4.14  | 6.77  | 5.76   | 7.38   | 6.81   | 5.92  | 4.56  | 6.47  | 7.09  | 7.23  | 4.32  | 6.04  | 5.80  | 6.96  | 4.97   | 4.57  | 7.12  | 7.22  |
| MnO                            | 0.11  | 0.10  | 0.13   | 0.16   | 0.13   | 0.20  | 0.11  | 0.14  | 0.15  | 0.15  | 0.05  | 0.16  | 0.16  | 0.10  | 0.20   | 0.13  | 0.12  | 0.19  |
| MgO                            | 25.85 | 8.59  | 11.98  | 19.53  | 12.48  | 10.62 | 8.34  | 10.72 | 14.90 | 12.44 | 6.84  | 7.93  | 11.50 | 8.74  | 8.44   | 9.82  | 9.97  | 4.06  |
| CaO                            | 5.01  | 3.60  | 7.66   | 6.20   | 5.70   | 7.05  | 8.95  | 7.13  | 6.77  | 7.55  | 17.12 | 11.66 | 8.99  | 2.57  | 15.24  | 10.21 | 5.58  | 2.97  |
| Na <sub>2</sub> O              | 0.77  | 1.82  | 2.22   | 2.36   | 1.77   | 1.48  | 1.52  | 1.10  | 1.71  | 1.46  | 1.97  | 1.35  | 0.84  | 1.74  | 2.22   | 1.87  | 1.28  | 1.79  |
| K <sub>2</sub> O               | 0.62  | 2.31  | 2.25   | 1.83   | 1.94   | 2.02  | 1.43  | 1.85  | 2.05  | 2.22  | 2.30  | 2.16  | 2.28  | 1.90  | 2.91   | 2.32  | 2.08  | 3.52  |
| P <sub>2</sub> O <sub>5</sub>  | 0.00  | 0.00  | 1.28   | 0.56   | 0.00   | 0.26  | 0.00  | 0.00  | 0.00  | 0.00  | 0.35  | 0.00  | 0.00  | 0.00  | 0.42   | 0.36  | 0.00  | 0.00  |
| Sum                            | 100   | 100   | 100    | 101    | 100    | 100   | 100   | 100   | 100   | 100   | 100   | 100   | 100   | 100   | 100    | 100   | 100   | 100   |
| B (ppm)                        | 52    | 68    | 202    | 184    | 104    | 61    | 32    | 61    | 96    | 69    | 108   | 78    | 62    | 53    | 149    | 71    | 53    | 61    |
| Cl                             | 2820  | 8515  | 15,057 | 13,382 | 10,508 | 5686  | 1210  | 3229  | 8650  | 7191  | 4295  | 3811  | 207   | 4281  | 11,267 | 9161  | 3440  | 7295  |
| Sc                             | < DL  | 26    | < DL   | < DL   | < DL   | < DL  | 31    | 13    | 7     | < DL  | 20    | 28    | 21    | 34    | < DL   | < DL  | 24    | 24    |
| Cr                             | 2880  | 568   | 523    | 1197   | 697    | 570   | 1118  | 844   | 1445  | 1027  | < DL  | < DL  | 824   | 1026  | < DL   | 444   | 1229  | < DL  |
| Ni                             | 1230  | 325   | < DL   | 353    | 585    | 396   | 574   | 791   | 1393  | 735   | < DL  | < DL  | < DL  | 240   | < DL   | < DL  | 826   | < DL  |
| Nd                             | 39    | 26    | 44     | 31     | 43     | 25    | 16    | 35    | 23    | 16    | 31    | 44    | 15    | 21    | 17     | 26    | < DL  | 39    |
| Sm                             | 2     | 3     | 3      | 2      | 3      | 3     | 2     | 3     | 3     | 2     | 2     | 4     | 3     | 3     | 2      | 2     | 3     | 4     |
| Gd                             | 1     | 3     | 3      | 1      | 2      | 3     | 2     | 3     | 2     | 3     | 3     | 4     | 3     | 4     | 2      | 3     | 4     | 5     |

**X-ray diffraction**

Most of the samples of both Umm an-Nar and Wadi Suq periods mainly contain quartz, feldspar and calcite in different proportions, while the Wadi Suq samples 049 and 055 make exception. Sample 049 stands apart due to the occurrence of pyroxene and abundant amphibole, probably actinolite, in addition to quartz. Sample 055 contains quartz, feldspar but also pyroxene (Fig. 11).

**Optical microscopy**

As already indicated by microCT, most of the samples of both Umm an-Nar and Wadi Suq periods show a fine-medium grain size and an oriented texture; several of them show abundant elongated voids (051, 052, 053, 055, 057, 058, 059, 060, 063 and 064), and vessels 049 and 055, attributed to the Wadi Suq period, are characterised by a coarse-grained paste (Fig. 12).

Regardless of the grain size and chronological attribution, the majority of the vessels contains lithic temper composed of

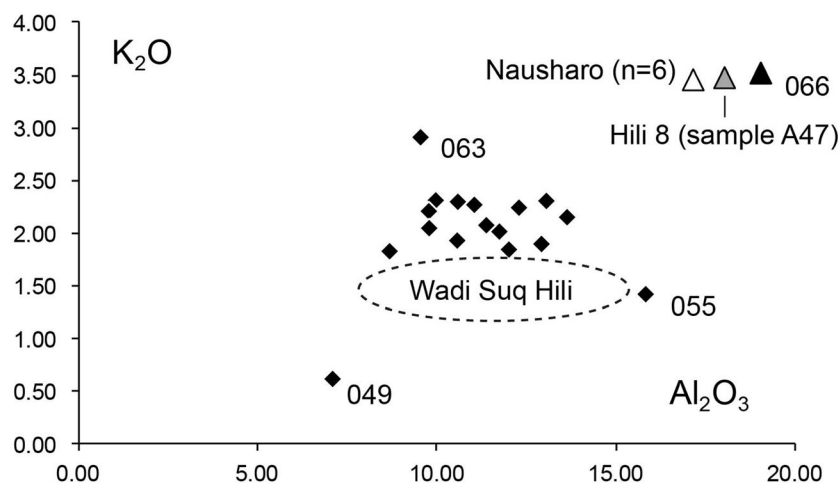
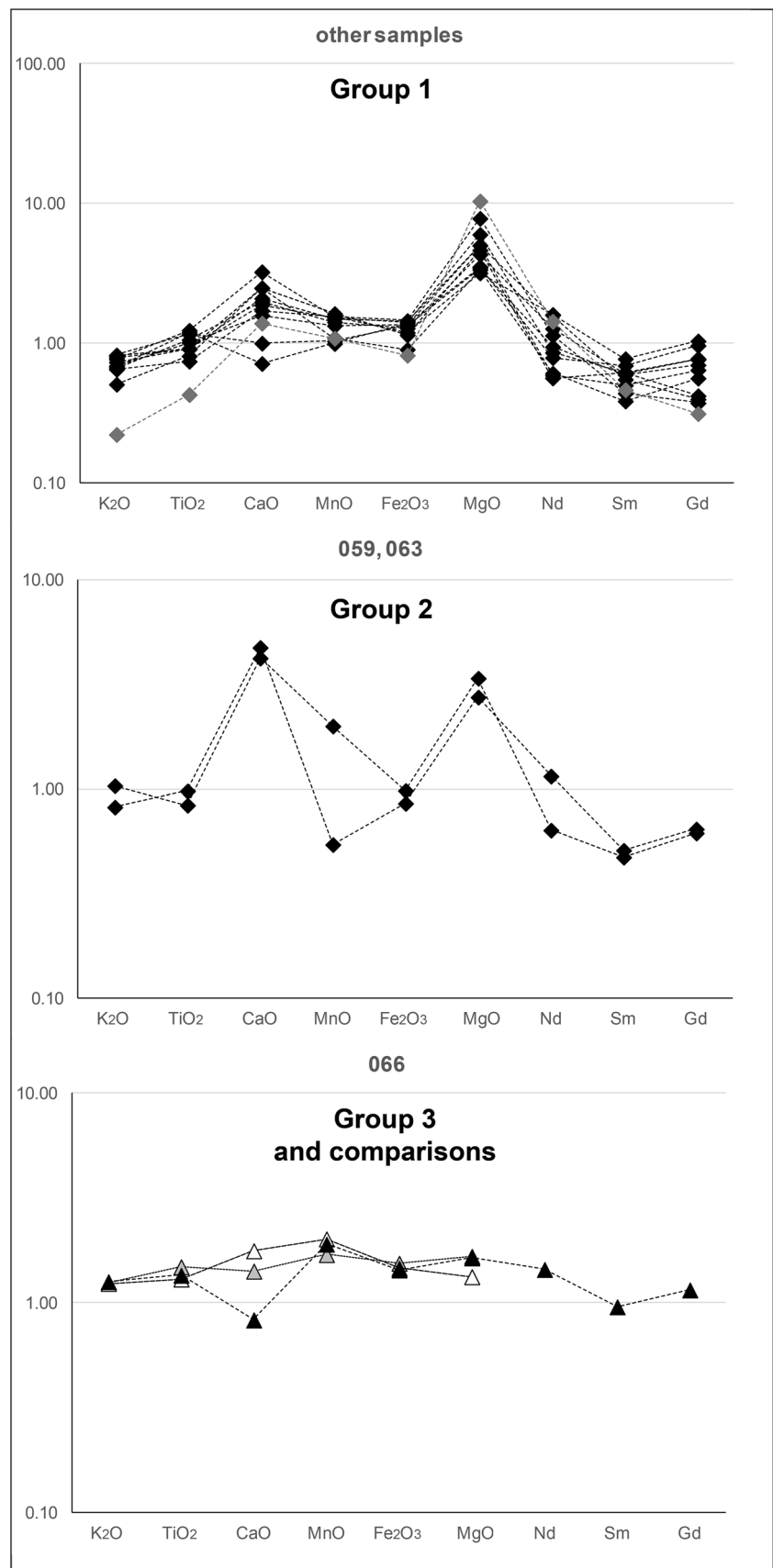


**Fig. 13** K<sub>2</sub>O vs. Al<sub>2</sub>O<sub>3</sub> bivariate diagram. Black diamonds correspond to the investigated samples of local origin; black triangle corresponds to sample 066; white triangle corresponds to the average composition of six black slipped jars from Nausharo (Pakistan; data taken from Bouquillon et al. 1996: p. 161, tab. 5); grey triangle corresponds to a

black slipped jar, sample A47, from Hili 8 (U.A.E.; data taken from Méry 2000: p. 234, tab. 63); dotted ellipse corresponds to compositional field of Wadi Suq coarse- and semi-fine-grained vessels from Hili (Méry 2000: pp. 250–257, tabs. 70–71, petrographic groups K, J, L)

**Fig. 14** The upper continental crust (UCC)-normalised spider diagrams of selected major and trace elements of the investigated vessels divided in 3 main groups. Trace element content has been multiplied by  $10^4$ . Grey diamonds in group 1 correspond to sample 049; white triangles in group 3 correspond to the average composition of six black slipped jars from Nausharo (Pakistan; data taken from Bouquillon et al. 1996: p. 161, tab. 5); grey triangles in group 3 correspond to a black slipped jar, sample A47, from Hili 8 (U.A.E.; data taken from Méry 2000: p. 234, tab. 63)





magmatic minerals and fragments of magmatic and low-grade metamorphic rocks (green schists). The recognised minerals include quartz, plagioclase, pyroxene, weathered olivine, serpentine and rare muscovite. The coarse-grained sample 055 shares similar phases but it contains abundant and large (up to 8–9 mm) gabbroic rock fragments, composed of pyroxene and plagioclase (Fig. 12). The other coarse-grained sample 049 is characterised by abundant large (length up to 3–4 mm) ophiolitic rock fragments, mainly composed of actinolitic amphiboles. Pyroxene, opaques and rare rock fragments are also present (Fig. 12).

Vessel 066, probably belonging to a jar imported from the Indus valley, stands apart from the others. It contains quartz, microcline, perthitic feldspar and rare plagioclase with a size generally between 0.1 and 0.3 mm. Other phases include abundant micas (both muscovite and biotite) and a few fragments of flint. Rare secondary carbonate fills few voids (Fig. 12).

### Prompt gamma activation analysis

The results of PGAA analysis, recalculated on a volatile-free basis, are reported in Table 3, while the data including LOI are reported in Supplementary Table 1.

To characterise the samples on the basis of their composition, as a first step,  $K_2O$  and  $Al_2O_3$  have been chosen, since they can be mainly correlated to the chemistry of the clay raw materials (Fig. 13). According to their  $K_2O$  and  $Al_2O_3$  content, regardless of their chronology and typology, most of the samples form one single well-clustered group. Very close to it, the sample 063 shows a similar  $Al_2O_3$  content but a slightly higher  $K_2O$  value (2.9 vs. about 2–2.5 wt%). As expected, considering the very peculiar coarse-grained textures shown by both microCT and optical microscopy, the Wadi Suq samples 049 and 055 have a quite different behaviour due to the scarcity of clay minerals and abundant presence of mafic phases. In particular, sample 049 is characterised by the lowest  $K_2O$  and  $Al_2O_3$  contents being mainly composed of metamorphic rock fragments deriving from a protolith rich in olivine and clinopyroxene, while sample 055 is  $Al_2O_3$  rich due to the presence of plagioclase.

Sample 066, probably belonging to a jar imported from the Indus valley, showing the highest  $Al_2O_3$  and  $K_2O$  contents (about 19 and 3.5wt%, respectively) is significantly different from all the other samples. Its high  $K_2O$  content is probably due to the peculiar occurrence of K-rich minerals, such as alkaline feldspars and micas more common in granitoid rock types.

In order to further differentiate the vessels, we have selected some of the most significant major and trace elements ( $K_2O$ ,  $TiO_2$ ,  $CaO$ ,  $MnO$ ,  $Fe_2O_3$ ,  $MgO$ , Nd, Sm and Gd) to produce spider diagrams (Fig. 14). Their concentration values have been normalised using the upper continental crust composition (Rudnick and Gao 2004), in order to enhance possible different geochemical

features; additionally, the contents of selected trace elements (i.e. Nd, Sm and Gd) have been multiplied by  $10^4$  to better visualise the data in the diagrams.

Investigated samples have been divided into three groups mainly considering the behaviour of  $CaO$  and  $MgO$  in the spider diagrams. This was done because (1) the  $MgO$  content is scarcely influenced by metamorphism, (2) the  $CaO$  content generally drops with the increase of metamorphism and (3) the  $CaO$  content can be also related to the presence of carbonate temper material within the paste.

Group 1 includes most of the investigated samples that, regardless of their grain size and chrono-typological attribution, share a comparable chemical composition. They contain abundant minerals deriving from variably metamorphosed ophiolitic sequences. According to such composition, in the spider diagrams (Fig. 14), we observe a uniform  $MgO$  peak, while the  $CaO$  content gradually varies probably in connection with variable metamorphic/magmatic modal ratios.

Group 2 includes the Wadi Suq samples 059 and 063 which show  $MgO$  values comparable with those of the first group but the  $CaO$  content is much higher due to the presence of carbonate temper material.

Finally, group 3 (Fig. 14) only includes sample 066, likely part of a jar imported from the Indus valley. Containing minerals most probably originated from a granitic area, it does not show the peaks of  $MgO$  and  $CaO$  and is characterised by a flat pattern approximately parallel to that one of the upper continental crust.

## Discussion and conclusions

MicroCT-derived data and their statistical analysis show that most of the investigated samples from Al-Khutim are characterised by fine to medium-grained pastes and were probably produced by using the wheel. The orientation of the pores would exclude both coiling and modelling techniques (Lindahl and Pikirayi 2010), while it is compatible with the adoption of slow and/or fast wheel. However, due to the small size of the samples, it is not possible to exclude that at least part of them was not produced by wheel throwing but by wheel shaping of coil-built roughouts. Such technique is well documented with slightly different variations at Umm an-Nar sites such as Salut and Hili (Méry 2000: p. 163; Méry et al. 2017: pp. 172–173).

Micro-structure of the investigated fine to medium-grained Wadi Suq shards, the presence of finger marks on their inner faces and technological data available for contemporary pottery assemblages from Hili and Shimal (Méry 2000: pp. 270–271) suggest that they were produced by wheel throwing.

Wadi Suq samples 049 and 055 are different from the others for their coarse-grained paste very rich in lithic inclusions. According to PCA results, sample 066 shows peculiar

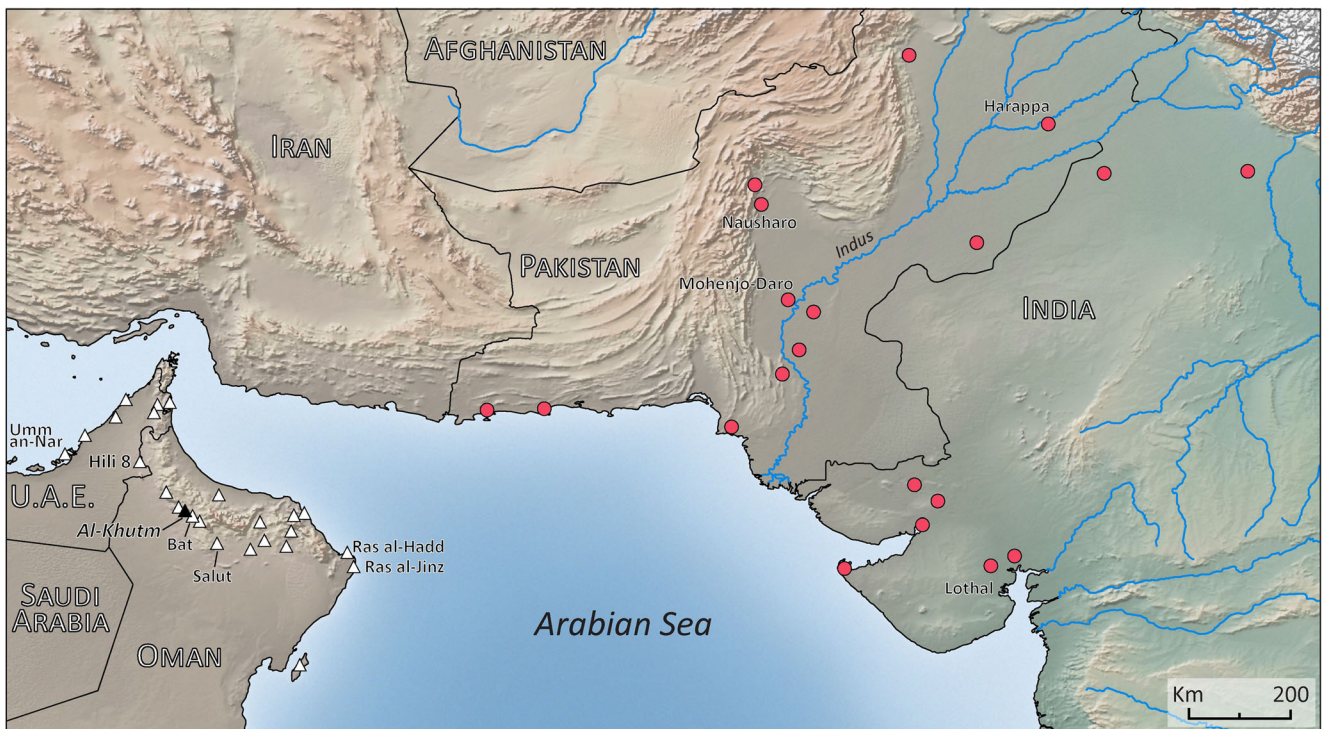


**Fig. 15** Distribution of BSJ (white triangles) in the Arabian peninsula and distribution of the main sites of the Indus civilization. Adapted from Méry 2000; Méry and Blackman 2000; Méry et al. 2017

technological features not comparable with those of the other vessels.

It is worth noting that while the Umm an-Nar fragments are generally featured by very fine- to medium-grained wares, the Wadi Suq ones are associated to a larger repertoire of shapes (beakers, bowls, jars, spouted jars) and characterised by a wider variability in paste grain size including also coarse-grained vessels. While a possible bias due the limited number of samples has to be considered, these data are in line with the macroscopic observation carried out on pottery from other towers at Bat (Thornton et al. 2016: pp. 179–208).

Mineralogical and petrographic data confirm the microCT results but, in addition, have revealed that all the samples, with the exception of vessel 066 and regardless of their grain size and typo-chronological attribution, share similar temper inclusions mainly composed of magmatic minerals and fragments of magmatic and low-grade metamorphic rocks (green schists). PGAA results further support such scenario. These vessels have, indeed, a similar chemical composition compatible with raw materials mainly deriving from ophiolitic complexes, sometime complemented with carbonate inclusions (samples 059, 063; Fig. 14). Since the Al-Khutm is located very close to such geological terrains, the collected data suggest a local production of most samples. Even if sampling local primary and secondary formations would be necessary to detail the raw material exploitation strategies adopted by the Al-Khutm groups, it is likely that the clay raw materials were

collected in surroundings of the site from late Tertiary and Quaternary deposits deriving from the erosion of the Al-Hajar Mountains and resulted in piedmont screes and alluvial fans (Minoux and Jaujon 1986; Desruelles et al. 2016).

The local production of most vessels is also confirmed by petrographic and chemical comparisons with contemporary pottery assemblages. Considering the Umm an-Nar period, the sandy red jars 050 and 060, the only investigated samples certainly belonging to such period beside the jar 066 (see below), are petrographically and chemically different from similar Hili productions (e.g.  $\text{SiO}_2$  content, about 56–63 vs. 68wt%—average composition of 4 vessels; Méry 2000: pp. 165–168, tab. 44, petrographic group B). Interestingly enough, samples 050 and 060 show petrographic features similar to those of a group of vessels from Umm an-Nar contexts (settlements and tombs) in the area of Bat and Amlah, close to Al-Khutm. They contain quartz, serpentine, olivine and other minerals most probably deriving from ultrabasic magmatic rocks belonging to ophiolitic complexes (Méry 2000: pp. 165–168, petrographic groups M, N, O). Overall, these data agree with the hypothesis that in this period, most of the pottery was locally produced and distributed (Méry 2000: p. 168).

Comparing the investigated Wadi Suq samples with contemporary coarse- and semi-fine-grained vessels from Hili (Méry 2000: pp. 250–257, tabs. 70–71, petrographic groups K, J, L), both groups contain ophiolitic material most probably

deriving from the Semail Nappe but the Al-Khutm vessels show a different  $K_2O$  vs.  $Al_2O_3$  ratio (Fig. 13). In addition, the petrographic composition of the Al-Khutm Wadi Suq samples is also different from that one of the Shimal contemporary productions, characterised by the absence of ophiolitic material (Méry 2000: pp. 264–265).

Sample 066 is a black slip wall fragment hypothetically attributed to the group of Indus black slipped jars (hereafter BSJ) characterised by a red micaceous paste (red-ware) and most probably originating from the Indus Basin (Blackman and Méry 1999; Méry and Blackman 2000, 2006). Available geochemical data suggest at least two most likely production areas corresponding to the Ravi and Indus rivers (Méry and Blackman 2006) in Pakistan. Micaceous red-ware vessels, including BSJ, were traded from the Indus area to Gujarat, Makrān, Baluchistan, Bahrain and south-eastern Arabia, including Oman, approximately from the second half of the third millennium BC (Blackman and Méry 1999; Méry and Blackman 2000, 2006; Méry et al. 2017).

Microtomographic, mineralogical, petrographic and chemical data obtained for sample 066 confirm such attribution. Its paste contains abundant micas (biotite and muscovite) and temper material, such as quartz, microcline, perthitic feldspar and rare plagioclase (with a size generally between 0.1 and 0.3 mm), compatible with an origin from a granitic area. These phases well correspond to those of BSJ even if amphiboles have not been identified in our sample. About one hundred analyses of BSJ by Instrumental Neutron Activation Analysis (INAA) are available but, unfortunately, just a few major elements have been published, limiting our possible comparisons with a few samples from the site Hili 8 in U.A.E. (Méry 2000) and Nausharo located in the interior of Baluchistan, Pakistan (obtained through XRF; Bouquillon et al. 1996). Nevertheless, the available data are enough to confirm the attribution of 066 to the BSJ group. In Fig. 13, sample A47 from Hili 8 and an average composition of six jars from Nausharo (hereafter Nausharo sample) plot very close to vessel 066 due to the high  $Al_2O_3$  and  $K_2O$  contents. As reported above, high  $K_2O$  contents are probably due to the peculiar occurrence of K-rich minerals, such as alkaline feldspars and micas. If the spider diagrams are considered (Fig. 14, group 3), samples 066, sample A47 from Hili 8 and the sample from Nausharo all show a flat pattern approximately parallel to that one of the upper continental crust. More in detail, the Hili 8 sample is particularly well comparable with sample 066, while Nausharo sample shows a slightly higher CaO content, perhaps due to the occurrence of carbonate temper material or secondary carbonate.

The occurrence of a BSJ at Al-Khutm integrates our knowledge about the presence of this type of vessels in Oman (Fig. 15) and indicates that during the Umm an-Nar period, the site was part of a long-distance connection system responsible for the distribution of BSJ.

Together with data collected from other Umm an-Nar sites like Bat and Salut (Thornton et al. 2016; Méry et al. 2017), this evidence confirms that the scale of the interaction between local communities and the Indus seafaring merchants was large and not restricted to the coastal sites but also involving the centres of the interior (Frenez et al. 2016; Frenez 2018).

Finally, from a methodological perspective, the combined use of microCT, PGAA and complementary destructive analysis (XRD, OM) has allowed a detailed characterisation of the investigated samples and has confirmed how microCT and the statistical analysis of microCT-derived data provide a precise description of pottery pastes highlighting possible differences between groups. When precious vessels, that cannot be sampled, have to be investigated, microCT, and chemical non-destructive analyses, such as XRF or PGAA, can be successfully applied to reconstruct the vessel-forming techniques and the provenance of the artefacts.

**Acknowledgements** We would like thank H.E. Hassan b. Mohammed Al-Lawati (Special Adviser for World Heritage Sites); Sultan b. Saif Al-Bakri, Director General for Archaeology; and Sultan b. Ali Al-Maqbali (Director World Heritage Sites Department) and Khamis Al-Asmi (Director Department of Excavations and Archaeological Studies) for giving us the opportunity to work at Al-Khutm. Special thanks to Sulaiman Hamood Aljabri (supervisor of Bat, Al-Khutm, and Al-Ayn) for his help and collaboration. We finally thank the Italian team working at Al-Khutm (Alessandro Armigliato, Marco Bianchi, Ilenia Gennuso, Antonio Di Michele) for the collection and preliminary analysis of the documentation of the pottery sample here presented.

**Author contributions** FB designed and led the study; FB, GV, ADM wrote the manuscript with contributions from all authors; FB, GV, EC, MC conducted archaeological research; GV, EC coordinated archaeological investigations; FB, LBS, ADM, DL, FP conducted mineralogical, petrographic and geochemical research with contributions from ZK and VS; FB, DP, CT conducted microCT scans and data analysis; ZK, VS, IH conducted PGAA; all authors contributed to final interpretation of data.

**Funding information** David Prokop has been financially supported by the Ministry of Education, Youth and Sports of the Czech Republic under the project CEITEC 2020 (LQ1601) and by the project CEITEC Nano Research Infrastructure (MEYS CR, 2016–2019). This research has been supported by Fondo Ricerca Ateneo 2018 of Trieste University in the framework of the project SCAN (Studio mineralogico, petrografico e strutturale di Ceramiche ANtiche tramite metodologie convenzionali e innovative). The PGAA measurements have been done at the Budapest Neutron Centre, within the IPERION CH project of the H2020-INFRAIA-2014-2015 framework, Grant Agreement No. 654028.

## References

- Anderson D (1995) Ceramic glaze analysis by simultaneous in-beam PGAA and XRFs. *J Radioanal Nucl Chem* 192(2):281–287
- ASTER NASA GDEM V3 = NASA/METI/AIST/Japan Space Systems, and U.S./Japan ASTER Science Team. ASTER global digital elevation model V003, 2018, distributed by NASA EOSDIS Land Processes DAAC, <https://doi.org/10.5067/ASTER/ASTGTM.003>.

- Belgja T, Révay ZS (2004) Gamma-ray spectrometry. In: Molnár GL (ed) Handbook of Prompt Gamma Activation Analysis with Neutron Beams. Kluwer Academic Publishers, Dordrecht/Boston/New York, pp 71–111
- Bernardini F, Tuniz C, Coppa A, Mancini L, Dreossi D, Eichert D, Turco G, Biasotto M, Terrasi F, De Cesare N, Hua Q, Levchenko V (2012) Beeswax as dental filling on a neolithic human tooth. *PLoS One* 7(9):e44904
- Bernardini F, De Min A, Lenaz D, Kasztovszky Z, Turk P, Velušček A, Szilágyi V, Tuniz C, Montagnari Kokelj E (2014a) Mineralogical and chemical constraints about the provenance of Copper Age polished stone axes of Ljubljana type from Caput Adriae. *Archaeom* 56(2):175–202
- Bernardini F, De Min A, Lenaz D, Kasztovszky Z, Turk P, Velušček A, Tuniz C, Montagnari Kokelj E (2014b) Petrographic and geochemical comparison between the Copper Age Ljubljana type axes and similar lithotypes from Eisenkappler Diabaszug complex (southern Austria). *J Archaeol Sci* 41:511–522
- Bernardini F, Vecchiet A, De Min A, Lenaz D, Mendoza Cuevas A, Gianoncelli A, Dreossi D, Tuniz C (2016) Neolithic pottery from the Trieste Karst (northeastern Italy): a multi-analytical study. *Microchem J* 124:600–607
- Bernardini F, Sibilía E, Kasztovszky Z, Boscutti F, De Min A, Lenaz D, Turco G, Micheli R, Tuniz C, Montagnari Kokelj M (2018) Evidence of open-air late prehistoric occupation in the Trieste area (North-Eastern Italy): dating, 3D clay plaster characterization and obsidian provenancing. *Archaeol Anthropol Sci* 10:1933–1943. <https://doi.org/10.1007/s12520-017-0504-7>
- Bernardini F, De Min A, Lenaz D, Kasztovszky ZS, Lughì V, Modesti V, Tuniz C, Tecchiati U (2019a) Polished stone axes from Varna/Nössingbühel and Castelrotto/Grondlboden, South Tyrol (Italy). *Archaeol Anthropol Sci* 11(4):1519–1531. <https://doi.org/10.1007/s12520-018-0612-z>
- Bernardini F, Leghissa E, Prokop D, Velušček A, De Min A, Dreossi D, Donato S, Tuniz C, Princivalle F, Montagnari Kokelj M (2019b) X-ray computed microtomography of Late Copper Age decorated bowls with cross-shaped foots from central Slovenia and the Trieste Karst (North-Eastern Italy): technology and paste characterisation. *Archaeol Anthropol Sci* 11:4711–4728. <https://doi.org/10.1007/s12520-019-00811-w>
- Blackman MJ, Méry S (1999) Les importations de céramiques harapéennes en Arabie orientale: état de la question. *Proceedings of the Semin for Arab Stud* 29:7–28
- Böhme M (2011) The Bat Type. A Hafit period tomb construction in Oman. *Arab Archaeol Epigr* 22(1):23–31
- Böhme M (2012) The recurring moment. Records on Hafit and Umm an-Nar period tomb architecture in the Oman Peninsula. In: Furrholt M, Hinz M, Mischka D (eds) *As time goes by?: monumentality, landscapes and the temporal perspective*. Verlag Dr. Rudolf Habelt GmbH, Bonn, pp 85–94
- Böhme M, Al-Sabri B (2011) Umm an-Nar burial 401 at Bat, Oman: architecture and finds. *Arab Archaeol Epigr* 22(2):113–154
- Bordet P, Courtois L (1967) Etude géologique des céramiques anciennes. Les techniques de fabrication *Comptes Rendus de l'Acad des Sci* 265:1665–1667
- Bouquillon A, Méry S, Schneider G, Quivron G (1996) Third millennium BC pottery at Nausharo (Pakistan): first results of a mineralogical and chemical program. *Archaeom*. 94. *Proceedings of the Int Symp on Archaeom* 29, Metu Ankara, Turkey, pp 151–168
- Brunswig RH (1989) Cultural history, environment and economy as seen from an Umm an-Nar settlement: evidence from test excavations at Bat, Oman 1977/78. *J Oman Studies* 1:109–112
- Cable CM (2012) A multitude of monuments: finding and defending access to resources in third millennium BC Oman. PhD Dissertation, Dept. of Anthropology, Michigan State University
- Cable CM, Thornton CP (2013) Monumentality and the third-millennium “towers” of the Oman Peninsula. In: Abraham S et al (eds) *Connections and complexity: new approaches to the archaeology*. Left Coast Press, Walnut Creek CA, pp 375–399
- Carter R (1997) *Defining the Late Bronze Age in Southeast Arabia: ceramic evolution and settlement during the second millennium BC*. PhD Dissertation, Institute of Archaeology, University College London
- Cattani M, Hassan al Lawati H, Sultan al Bakri S, Tosi M, Cocca E, Armigliato A, Mantellini S, Vinci G (2017) The excavation at the Bronze Age tower of Al-Khutm (Bat, Sultanate of Oman): a preliminary evaluation of the monument. *Proceedings of the Sem for Arab Stud* 47:51–56
- Charbonnier J (2015) Groundwater management in Southeast Arabia from the Bronze Age to the Iron Age: a critical reassessment. *Water Hist* 7:39–71
- Choi HD, Firestone RB, Lindstrom RM, Molnár GL, Mughabghab SF, Paviotti-Corcuera R, Révay ZS, Trkov A, Zerkin V, Chunmei Z (2007) Database of prompt gamma rays from slow neutron capture for elemental analysis. International Atomic Energy Agency, Vienna. <https://www.iaea.org/publications/7030/database-of-prompt-gamma-rays-from-slow-neutron-capture-for-elemental-analysis>. Accessed 28 February 2020
- Cleuziou S (1989a) Excavations at Hili 8: a preliminary report on the 4th to 7th campaigns. *Archaeol in the United Arab Emirates* 5:61–88
- Cleuziou S (1989b) The chronology of protohistoric Oman as seen from Hili. In: Costa PM, Tosi M (eds) *Oman studies, papers on the archaeology and history of Oman*, Ist. Ital. per il Medio ed Estremo Oriente 63, Roma, pp 47–78
- Cleuziou S, Tosi M (2007) In the shadow of the ancestors. The prehistoric foundations of the early Arabian civilization in Oman. Ministry of Heritage and Culture Sultanate of Oman, Muscat
- Cocca E, Vinci G, Cattani M, Armigliato A, Di Michele A, Bianchi M, Gennuso I (2019) Al-Khutm project 2017/2018: a Bronze Age monumental tower (Bat, Oman). *Proceedings of the Sem for Arab Stud* 49:85–96
- Courty MA, Roux V (1995) Identification of wheel throwing on the basis of ceramic surface features and microfibrils. *J Archaeol Sci* 22:17–50
- Cremaschi M, Esposti MD, Fleitmann D, Perego A, Sibilía E, Zerboni A (2018) Late Holocene onset of intensive cultivation and introduction of the falaj irrigation system in the Salut oasis (Sultanate of Oman). *Quat Sci Rev* 200:123–140. <https://doi.org/10.1016/j.quascirev.2018.09.029>
- Crupi V, Zs K, Khalilli F, La Russa MF, Macchia A, Majolino D, Rossi B, Rovella N, Ruffolo SA, Venuti V (2016) Evaluation of complementary methodologies applied to a preliminary archaeometric study of glazed pottery from Aghs (Azerbaijan). *International Journal of Conservation Science* 7(2):901–912
- de Cardi B, Collier S, Doe DB (1976) Excavations and survey in Oman, 1974–1975. *J Oman Studies* 2:101–75
- Desruelles S, Fouache E, Eddargach W, Cammas C, Wattez J, Beuzen-Waller T, Martin C, Tengberg M, Cable C, Thornton C, Murray A (2016) Evidence for early irrigation at Bat (Wadi Sharsah, north-western Oman) before the advent of farming villages. *Quat Sci Rev* 150:42–54
- Döpfer S (2018) Towers and ditches in third millennium BC Eastern Arabia: a view from Building II at Bat. *Paléorient* 44(1):121–133
- Döpfer S, Schmidt C (2014) German expedition to Bat and Al Ayn, Sultanate of Oman: the 2010 to 2013 seasons. *J Oman Studies* 18: 187–230
- Duches R, Nannini N, Fontana A, Boschin F, Crezzini J, Bernardini F, Tuniz C, Dalmeri G (2019) Archeological bone injuries by lithic backed projectiles: new evidence on bear hunting from the Late Epigravettian site of Cornafessa rock shelter (Italy). *Archaeol*

- Anthropol Sci 11(5):2249–2270. <https://doi.org/10.1007/s12520-018-0674-y>
- Frenéz D (2018) The Indus Civilization trade with the Oman Peninsula. In: Cleuziou S, Tosi M In the Shadow of the Ancestors. The Prehistoric Foundations of the Early Arabian Civilization in Oman, Ministry of Heritage and Culture, Sultanate of Oman, 2nd expanded edition, pp 385–397
- Frenéz D, Degli Esposti M, Méry S, Kenoyer JM (2016) Bronze Age Salut (ST1) and the Indus Civilization: recent discoveries and implications. *Proceedings of the Sem for Arab Stud* 46:107–124
- Frifelt K (1975) On prehistoric settlement and chronology of the Oman Peninsula. *East and West* 25(3/4):359–424
- Frifelt K (1976) Evidence of a third millennium BC town in Oman. *J Oman Stud* 2:57–74
- Frifelt K (1985) Further evidence of the third millennium BC town at Bat in Oman. *J Oman Stud* 7(1):89–104
- Frifelt K (2002) Bat, a center in third millennium Oman. In: Cleuziou S, Tosi M, Zarins J (eds) *Essays on the Late Prehistory of the Arabian Peninsula*. *Ist Ital per l’Africa e l’Oriente*, Roma, pp 101–110
- Gentelle P, Frifelt K (1989) About the distribution of third millennium graves and settlements in the Ibbri Area of Oman. In: Costa PM, Tosi M (eds) *Oman studies: papers on the archaeology and history of Oman*. *Ist Ital per il Medio Ed Estremo Oriente*, Rome, pp 116–119
- Jasim SA (2012) The necropolis of Jebel Buhais: prehistoric discoveries in the Emirate of Sharjah United Arab Emirates. The Department of Culture & Information, Government of Sharjah, UAE
- Jolliffe IT (2002) *Principal component analysis*, 2nd edn. Springer, New York
- Kahl W-A, Ramminger B (2012) Non-destructive fabric analysis of prehistoric pottery using high-resolution X-ray microtomography: a pilot study on the late Mesolithic to Neolithic site Hamburg-Boberg. *J Archaeol Sci* 39:2206–2219
- Kassambara A (2017) Practical guide to principal component methods in R. *STHDA*. <https://payhip.com/b/shrk>. Accessed 28 February 2020
- Kasztovszky ZS (2007) Application of prompt gamma activation analysis to investigate archaeological ceramics. *Archeometria Műhely IV/2*: 49–54. <http://www.ace.hu/am/>. Accessed 28 February 2020
- Kasztovszky ZS, Antczak MM, Antczak A, Millan B, Bermúdez J, Sajo-Bohus L (2004) Provenance study of Amerindian pottery figurines with prompt gamma activation analysis. *Nukleonika* 49(3):107–113
- Kasztovszky ZS, Biró KT, Markó A, Dobosi V (2008) Cold neutron prompt gamma activation analysis – a non-destructive method for characterisation of high silica content chipped stone tools and raw materials. *Archaeom* 50(1):12–29
- Kasztovszky Z, Maróti B, Harsányi I, Párkányi D, Szilágyi V (2018) A comparative study of PGAA and portable XRF used for non-destructive provenancing archaeological obsidian. *Quat Int* 468: 179–189
- Kozatsas J, Kotsakis K, Sagris D, David K (2018) Inside out: assessing pottery forming techniques with micro-CT scanning. An example from Middle Neolithic Thessaly. *J Archaeol Sci* 100:102–119
- Laursen and Steinkeller (2017) *Babylonia, the Gulf Region and the Indus*. Archaeological and Textual Evidence for Contact in the Third and Early Second Millennia BC. Eisenbrauns, Winona Lake
- Leghissa E, Kasztovszky Z, Szilágyi V, Harsányi I, De Min A, Princivalle F, Montagnari Kokelj M, Bernardini F (2020) Late-Copper-Age decorated bowls from the Trieste Karst (north-eastern Italy): what can typology, technology and non-destructive chemical analyses tell us on local vs. foreign production, exchange systems and human mobility patterns? *Quat Int* 539:92–104
- Leigh B (2016) Metal. In: Thornton CP, Cable CM, Possehl GL (eds) *The bronze age towers at Bat, Sultanate of Oman*. Research by the Bat Archaeological Project. University of Pennsylvania, Philadelphia, pp 2007–2012
- Lenaz D, Adetunji J, Rollinson H (2014) Determination of Fe<sup>3+</sup>/ΣFe ratios in chrome spinels using a combined Mössbauer and single-crystal X-ray approach: application to chromitites from the mantle section of the Oman ophiolite. *Contributions to Mineralogy and Petrology* 167, article 958, DOI <https://doi.org/10.1007/s00410-013-0958-2>
- Lindahl A, Pikirayi I (2010) Ceramics and change: an overview of pottery production techniques in northern South Africa and eastern Zimbabwe during the first and second millennium AD. *Archaeol Anthropol Sci* 2(3):133–149
- Machado AS, Oliveira DF, Gama Filho HS, Latini R, Bellido AVB, Assis JT, Anjos MJ, Lopes RT (2017) Archeological ceramic artifacts characterization through computed microtomography and X-ray fluorescence. *X-Ray Spectrom*. <https://doi.org/10.1002/xrs.2786>
- Magee P (2014) *The archaeology of prehistoric Arabia: adaptation and social formation from the Neolithic to the Iron Age*. Cambridge University Press, New York
- Mantellini S (2015) Al-Khutn excavation. 31 October – 3 December 2015. Unpublished report submitted to the Ministry of Heritage and Culture, Sultanate of Oman
- Méry S (2000) Les céramiques d’Oman et l’Asie moyenne. Une archéologie des échanges à l’Âge du Bronze. CNRS, Paris
- Méry S, Blackman MJ (2000) Harappa et Mohenjo- Daro: deux zones de production de jarres à engobe noir au Pakistan à la Période Indus. *Paléorient* 25(2):167–177
- Méry S, Blackman MJ (2006) Socio-economical patterns of a ceramic container: the Harappan Black Slipped Jar. In: Jarrige C, Lefèvre V (eds) *Sixteenth International Conference on South Asian Archaeology*. Éditions Recherche sur les Civilisations, Paris, pp 226–235
- Méry S, Degli Esposti M, Frenéz D, Kenoyer JM (2017) Indus potters in central Oman in the second half of the third millennium BC. First results of a technological and archaeometric study. *Proceedings of the Sem for Arab Stud* 47:163–184
- Minoux L, Jaujon D (1986) Geological map of Ibbri, Oman. Sheet NF 40-2F, 1:100,000, Ministry of Petroleum and Minerals, Muscat
- Palamara E, Zacharias N, Xanthopoulou M, Zs K, Kovács I, Palles D, Kamitsos EI (2016) Technology issues of Byzantine glazed pottery from Corinth, Greece. *Microchem J* 129:137–150
- Prokop D (2018) Processing of tomographic data by principal component analysis method for archaeological applications. Master’s thesis, Brno University of Technology
- Révay ZS (2009) Determining elemental composition using prompt gamma activation analysis. *Anal Chem* 81:6851–6859
- Révay ZS, Belgya T, Molnár GL (2005) Application of Hypermet-PC in PGAA. *J Radioanal Nucl Chem* 265:261–265
- Righetti S (2015) Les cultures du Wadi Suq et de Shimal dans la péninsule omanaise au II<sup>ème</sup> millénaire avant notre ère. Évolution des sociétés du Bronze moyen et du Bronze récent. PhD dissertation, Université Paris 1 Panthéon-Sorbonne
- Righetti S, Cleuziou S (2010) The Wadi Suq pottery: a typological study of the pottery assemblage at Hili 8 (UAE). *Proceedings of the Sem for Arab Stud* 40:283–292
- Rudnick RL, Gao S (2004) Composition of continental crust. In: Holland HD, Turekian KK (eds) *Treatise on Geochemistry*. Elsevier, V. 3 (The Crust), pp 1–64
- Rye OS (1977) Pottery manufacturing techniques: X-ray studies. *Archaeom* 19:205–211
- Sanger MC (2016) Investigating pottery vessel manufacturing techniques using radiographic imaging and computed tomography: studies from the Late Archaic American Southeast. *J Archaeol Sci Rep* 9: 586–598
- Schmidt C, Döpper S (2016) Umm an-Nar pottery assemblages from Bat and al-Zibya and their functional contexts. *Proceedings of the Sem for Arab Stud* 46:247–262
- Sekimoto S, Saito Y, Ito D, Homura Y, Ebihara M, Kawabata Y (2013) Attempts for simultaneous observation of image and elemental

- component in a pottery sample using neutrons. *Phys Procedia* 43: 352–359
- Soret M, Agard P, Dubacq B, Plunder A, Yamato P (2017) Petrological evidence for stepwise accretion of metamorphic soles during subduction infancy (Semail ophiolite, Oman and UAE). *J Metamorph Geol* 35:1051–1080
- Sueki K, Oura Y, Sato W, Nakahara H, Tomizawa T (1998) Analysis of archaeological samples by the internal monostandard method of PGAA. *J Radioanal Nucl Chem* 234:2–31
- Szakmány G, Kasztovszky Z, Szilágyi V, Stamini E, Friedel O, Biró KT (2011) Discrimination of prehistoric polished stone tools from Hungary with non-destructive chemical prompt gamma activation analyses (PGAA). *Eur J Mineral* 23:883–893
- Szentmiklósi L, Belgya T, Révay ZS, Kis Z (2010) Upgrade of the prompt gamma activation analysis and the neutron-induced prompt gamma spectroscopy facilities at the Budapest Research Reactor. *J Radioanal Nucl Chem* 286:501–505
- Szilágyi V, Gyarmati J, Tóth M, Taubald H, Balla M, Zs K, Gy S (2012) Petro-mineralogy and geochemistry as tools of provenance analysis on archaeological pottery: study of Inka Period ceramics from Paria, Bolivia. *J S Am Earth Sci* 36:1–17
- Thornton CP, Schmidt C (2015) The UNESCO World Heritage Site of Bat and Al-Ayn: past, present and future. In: al-Lawati HMA (ed) *The Archaeological Heritage of Oman* (UNESCO), Proceedings of the Symposium (Paris-September 7th, 2012). Ministry of Heritage and Culture, Muscat, pp 155–63
- Thornton CP, Cable CM, Possehl GL (2016) The bronze age towers at Bat, Sultanate of Oman. Research by the Bat Archaeological Project 2007–2012. University of Pennsylvania, Philadelphia
- Tuniz C, Bernardini F, Turk I, Dimkaroski L, Mancini L, Dreossi D (2012) Did neanderthals play music? X-ray computed microtomography of the Divje babe ‘flute’? *Archaeometry* 54:581–590
- Tuniz C, Bernardini F, Cicuttin A, Crespo ML, Dreossi D, Gianoncelli A, Mancini L, Mendoza Cuevas A, Sodini N, Tromba G, Zanini F, Zanolli C (2013) The ICTP-Elettra X-ray laboratory for cultural heritage and archaeology. *Nucl Instrum Methods Research Sec A* 711:106–110
- Velde C (2003) Wadi Suq and Late Bronze Age in the Oman Peninsula. In: Potts DT, Al Naboodah H, Hellyer P (eds) *Archaeology of the United Arab Emirates*. Trident Press, London, pp 102–113
- Vogt B, Franke-Vogt U (eds) (1987) *Shimal 1985/1986*. Excavations of the German Archaeological Mission in Ras al-Khaimah, U.A.E. A preliminary report. Reimer Verlag, Berlin

**Publisher's note** Springer Nature remains neutral with regard to jurisdictional claims in published maps and institutional affiliations.